A&A 622, A138 (2019)
https://doi.org/10.1051/0004-6361/201832728

Astronomy & Astrophysics

Four GRB supernovae at redshifts between 0.4 and 0.8

The bursts GRB 071112C, 111228A, 120714B, and 130831A*

S. Klose[1], S. Schmidl[1], D. A. Kann[1,2], A. Nicuesa Guelbenzu[1], S. Schulze[3,4,5], J. Greiner[6], F. Olivares E.[5,7], T. Krühler[6], P. Schady[6], P. M. J. Afonso[8], R. Filgas[9], J. P. U. Fynbo[10], A. Rau[6], A. Rossi[11], K. Takats[5], M. Tanga[6], A. C. Updike[12], and K. Varela[6]

(Affiliations can be found after the references)

Received 29 January 2018 / Accepted 19 November 2018

ABSTRACT

Twenty years ago, GRB 980425/SN 1998bw revealed that long gamma-ray bursts (GRBs) are physically associated with broad-lined type-Ic supernovae (SNe). Since then more than 1000 long GRBs have been localized to high angular precision, but only in ~50 cases has the underlying SN component been identified. Using the Gamma-Ray Burst Optical Near-Infrared Detector (GROND) multi-channel imager at ESO/La Silla, during the last ten years we have devoted a substantial amount of observing time to reveal and study SN components in long-GRB afterglows. Here we report on four more GRB SNe (associated with GRBs 071112C, 111228A, 120714B, and 130831A) which were discovered and/or followed-up with GROND and whose redshifts lie between $z = 0.4$ and 0.8. We study their afterglow light curves, follow the associated SN bumps over several weeks, and characterize their host galaxies. Using SN 1998bw as a template, the derived SN explosion parameters are fully consistent with the corresponding properties of the currently known GRB-SN ensemble, with no evidence for an evolution of their properties as a function of redshift. In two cases (GRB 120714B/SN 2012eb at $z = 0.398$ and GRB 130831A/SN 2013fu at $z = 0.479$) additional Very Large Telescope (VLT) spectroscopy of the associated SNe revealed a photospheric expansion velocity at maximum light of about 40 000 and 20 000 km s^{-1}, respectively. For GRB 120714B, which was an intermediate-luminosity burst, we find additional evidence for a black-body component in the light of the optical transient at early times, similar to what has been detected in some GRB SNe at lower redshifts.

Key words. gamma-ray burst: individual: GRB 071112C – gamma-ray burst: individual: GRB 111228A – supernovae: individual: SN 2013fu – gamma-ray burst: individual: GRB 130831A – supernovae: individual: SN 2012eb – gamma-ray burst: individual: GRB 120714B

1. Introduction

The association of SN 1998bw in the spiral galaxy ESO 184-G82 ($z = 0.0085$, Tinney et al. 1998) with the long GRB 980425 (Galama et al. 1998) provided the first clue that long-duration GRBs are associated with the deaths of massive stars. Twenty years after SN 1998bw there is mounting observational and theoretical evidence that long GRBs have their origin in a subclass of broad-lined type-Ic supernovae (SNe), which spectroscopically reveal high expansion velocities (for reviews see, e.g., Cobb 2012; Hjorth & Bloom 2012; Hjorth 2013; Cano et al. 2017). Since long GRBs signal the explosions of massive stars, they potentially allow for a zoom-in into the high-z universe at times when Population III stars formed and exploded (e.g., Mesler et al. 2014).

Currently, there are approximately 50 known GRB SNe, which were discovered photometrically as a late-time bump in GRB afterglows, but there has been spectroscopic confirmation for only half of these (Cano et al. 2017). At least some might be linked to the formation of a magnetar (e.g., Mazzali et al. 2014; Greiner et al. 2015; Kann et al. 2016; Lü et al. 2018), potentially even including SN 1998bw (Wang et al. 2017). Supernova bumps have been detected up to a redshift of $z = 1.06$ (GRB 000911; Masetti et al. 2005) and spectroscopically studied up to $z = 1.01$ (GRB 021211/SN 2002lt; Della Valle et al. 2003a,b). For two decades, GRB 980425/SN 1998bw has remained the closest GRB SN detected. As such it is also the best-studied GRB-SN event and is therefore used as the standard template for basically all GRB-SN studies in the optical bands (Zeh et al. 2004; Cano 2013).

In the pre-*Swift* (*Neil Gehrels Swift* Observatory) satellite (Gehrels et al. 2004) era (1997–2004) the annual discovery rate of long-GRB afterglows with a redshift $z < 1$ (< 0.5), that is, those potentially suited for GRB-SN detections, was on average about 2–3 (1–2) events per year. In the *Swift* era (2005+) this rate increased to about 6–8 (3–4) per year (no $z < 0.5$ burst in 2007, and only 1 burst in 2008 and 2014), while the discovery rate of the accompanying GRB SNe settled at on average 1 to 2 events per year. For $0.5 < z < 1.0$, visibility constraints and substantial observational efforts for a required photometric long-term follow up might be the main reasons why most GRB SNe were missed, though in some cases host-galaxy extinction (e.g., Soderberg et al. 2006) or an intrinsically faint SN (e.g., Niino et al. 2012, but see de Ugarte Postigo et al. 2018) might have played a role too.

One could also speculate that a long-lasting bright optical afterglow could hide a rising SN component (thanks to the referee for pointing this out). Indeed, this was the case for GRB 030329; here the R_c-band light curve did not show a bump since the transition between afterglow light and SN light was very smooth (see Fig. 3 in Zeh et al. 2005a). Though a detailed

* Based on observations collected with GROND at the MPG 2.2 m telescope at ESO La Silla Observatory (PI: J. Greiner), the Very Large Telescope of the European Southern Observatory, Paranal Observatory, Chile (ESO programme 092.A-0231B, PI: T. Krühler), Keck LRIS and MOSFIRE (PI: D. A. Perley), *Spitzer* (PI: D. A. Perley), and publicly available data obtained from the Gemini, *Hubble* Space Telescope (HST), and Telescopio Nazionale *Galileo* (TNG) data archives.

investigation of this possibility remains to be carried out, *ad hoc* it appears to be a less likely situation. On the one hand, at least the GROND data archive always includes multi-color data. This might strongly reduce the probability of missing a rising SN component. On the other hand, once information on redshift was available and $z \lesssim 0.5$ found, spectroscopic observations were very likely triggered by the GRB community.

At redshifts $z \lesssim 0.1$, observational efforts to monitor an expected/accompanying SNe were usually high and led to the discovery of thermal components in early GRB afterglows (e.g., Campana et al. 2006; Olivares et al. 2012; Starling et al. 2012; Schulze et al. 2014) and allowed for detailed studies of the SN explosion parameters (for a review see Cano et al. 2017, and references therein). Moreover, this led to the discovery of three events where no underlying SN component was found down to deep flux limits (GRB 060505 at $z = 0.089$ and GRB 060614 at $z = 0.125$: e.g., Della Valle et al. 2006; Fynbo et al. 2006; Gal-Yam et al. 2006; Xu et al. 2009; as well as GRB 111005A at $z = 0.01326$: Michałowski et al. 2018; Tanga et al. 2018). This has raised the question of whether some long bursts could have their origin in failed SNe which immediately collapse into a black hole. The low redshift of these well-studied SNe also allowed for detailed studies of their host galaxies (e.g., Fynbo et al. 2012a; Thöne et al. 2014; Izzo et al. 2017; Krühler et al. 2017), including the host of the GRB-SN prototype SN 1998bw (Michałowski et al. 2012, 2018). Though, even for events at higher redshifts detailed host-galaxy studies have been performed (de Ugarte Postigo et al. 2018).

The relatively small annual discovery rate of GRB SNe calls for detailed follow-up observations of each event. While spectroscopic observations usually need the biggest telescopes in order to get a reasonable signal-to-noise ratio, photometric studies are less demanding and can be performed using smaller telescopes as well.

Here we report on observations of a further set of four GRB SNe observed with GROND (MPG 2.2 m, ESO/La Silla; Greiner et al. 2007, 2008) in the optical/near-infrared(NIR) bands in the years between 2007 and 2013. Previous results of follow-up observations of GRB SNe with GROND were presented in Olivares et al. (2012; GRB/XRF 100316D/SN 2010bh), Olivares et al. (2015; GRBs 081007/SN 2008hw, 091127/SN 2009nz, 101219B/SN 2010ma), as well as Greiner et al. (2015) and Kann et al. (2016; GRB 111209A/SN 2011kl). Three of the events discussed here are studied for the first time (GRBs 071112C, 111228A, 120714B), while GRB 130831A/SN 2013fu was also explored by Cano et al. (2014) using an independent data set. Two of the events we study could also be investigated based on spectroscopic follow-up campaigns with the Very Large Telescope (GRB 120714B/SN 2012eb, GRB 130831A/SN 2013fu; Klose et al. 2012a,b, 2013a,b).

The paper is organized as follows. We start with a brief overview concerning the observational details (Sect. 2) and then focus on the SN light curves (Sect. 3.1). Thereafter, we report (i) on the results of our early-time VLT/X-shooter spectroscopy of the optical transient that followed GRB 120714B (Sect. 3.3) and (ii) on the results of the VLT/FORS2 (FOcal Reducer and low dispersion Spectrograph) spectroscopy around SN maximum (GRB 120714B/SN 2012eb and GRB 130831A/SN 2013fu; Sect. 3.2). In Sect. 4 we derive the relevant explosion parameters of the SNe and put the properties of the four GRB SNe in the context of the full presently known sample. of well-observed GRB SNe. In addition, we summarize the properties of the corresponding afterglows and GRB host galaxies.

In the following, we use the convention $F_\nu(t) \sim t^{-\alpha}\nu^{-\beta}$ to describe the temporal and spectral evolution of the flux density $F_\nu(t)$ of an afterglow. We use a ΛCDM cosmology with $H_0 = 71\,\mathrm{km\,s^{-1}\,Mpc^{-1}}$, $\Omega_\mathrm{M} = 0.27$, and $\Omega_\Lambda = 0.73$ (Spergel et al. 2003).

2. Observations and data reduction

2.1. GROND multi-color imaging

The multi-color GROND data were reduced in a standard fashion (bias subtraction, flat fielding, co-adding) with a customized pipeline (for details see Krühler et al. 2008; Yoldaş et al. 2008) which is based on standard routines in `IRAF` (Image Reduction and Analysis Facility; Tody 1986). To measure the brightness of the optical/NIR transient we employed aperture photometry as well as point-spread-function (PSF) photometry using the DAOPHOT and ALLSTAR packages in `IRAF` (Tody 1993), similar to the procedure described in Krühler et al. (2008) and Yoldaş et al. (2008). Once an instrumental magnitude was established, it was photometrically calibrated against the brightness of a number of field stars measured in a similar manner.

PSF photometry was used when the afterglow dominated the light of the optical transient at early times (GRBs 071112C, 111228A, and 130831A), while aperture photometry was always applied for the fainter SN and host-galaxy component. In the case of the GRB 120714B the afterglow, the SN, and the host were of similar brightness, and therefore aperture photometry was used. Since all four host galaxies turned out to be either compact on our images (GRBs 071112C, 111228A, and 120714B) or very faint (GRBs 071112C, 111228A, and 130831A), and since in all cases the afterglow/SN was situated well within the light of the host, there is no mismatch between PSF and aperture photometry even though we did not perform image subtraction against a late-time reference image.

Photometry was tied to the Sloan Digital Sky Survey (SDSS) DR7 catalog (Abazajian et al. 2009) in the optical filters ($g'r'i'z'$) and the Two-Micron All Sky Survey (2MASS; Skrutskie et al. 2006) in the NIR bands (JHK_s). Details on the GROND extinction corrections and Vega–AB conversions can be found in, for example, Rossi et al. (2012), and central wavelengths of the GROND filter bands are listed in, for example, Rossi et al. (2011).

2.2. Late-time host-galaxy imaging using other telescopes

Late-epoch, host-galaxy imaging data using other instruments than GROND were obtained with the High Acuity Wide-field K-band Imager (HAWK-I) at ESO/VLT on ESO/Paranal, DoLoRes (Device Optimized for LOw RESolution) mounted at the Telescopio Nazionale *Galileo* (TNG), La Palma, the Gemini Multi-Object Spectrographs (GMOS) at the Frederick C. Gillett Gemini North telescope on Mauna Kea, the Low Resolution Imaging Spectrometer (LRIS) mounted at Keck I on Mauna Kea, and the Infrared Array Camera (IRAC) at the *Spitzer* Space Telescope.

Gemini raw data were downloaded from the Gemini archive[1], TNG raw data from the TNG archive[2]. Keck data stem from SHOALS (Perley et al. 2016a,b), *Spitzer*/IRAC data from the *Spitzer* GRB host galaxy data base (Perley et al. 2016c).

[1] https://archive.gemini.edu/
[2] http://ia2.oats.inaf.it/archives/tng

All data were reduced in a standard fashion using IRAF (Tody 1986). In all cases, host-galaxy magnitudes were obtained by aperture photometry. Optical data were calibrated against field stars from the SDSS DR 12 catalog (Alam et al. 2015) and near-infrared data were calibrated against the Two Micron All Sky Survey (Skrutskie et al. 2006). The transformations proposed by Lupton et al. (2005) were used to transform SDSS into R_c and I_c-band magnitudes.

2.3. Ultraviolet Optical Telescope imaging of GRB 111228A

We expand our photometric database of GRB 111228A by adding the Ultraviolet Optical Telescope (UVOT; Roming et al. 2005) observations from the *Neil Gehrels Swift* Observatory. Photometry with UVOT was carried out on pipeline-processed sky images downloaded from the *Swift* data center[3] following the standard UVOT procedure (Poole et al. 2008). Source photometric measurements were extracted from the UVOT early-time event data and later imaging data files using the tool UVOTMAGHIST (v1.1) with a circular source extraction region of 3.″5 to maximize the S/N. In order to remain compatible with the effective area calibrations, which are based on 5″ aperture photometry (Poole et al. 2008), an aperture correction was applied. At late times, in each filter, we stacked all observations that had only yielded upper limits to achieve deeper constraints on the SN/host galaxy. No detections were made in these deep stacks.

2.4. Light-curve analysis

Parameters of GRB SNe were extracted using an analytical ansatz which expresses the light of the optical transient (OT) as the sum of afterglow light (AG), host-galaxy light, and light from an underlying SN component. The flux density, F_ν, in a given photometric band that is characterized by its frequency ν is then given by (Zeh et al. 2004, 2005b)

$$F_\nu^{\rm OT}(t) = F_\nu^{\rm AG}(t) + k\,F_\nu^{\rm SN}(t/s) + F_\nu^{\rm host}, \quad (1)$$

where the parameter k describes the observed luminosity ratio between the GRB SNe at peak time, and the SN template in the considered band (in the observer frame). The parameter s is a stretch factor with respect to the used template. Thereby, if $s < 1$ ($s > 1$), the SN is developing faster (slower) than the template GRB SN. Following almost all GRB-SN studies, the template used here is SN 1998bw (Galama et al. 1998), though other template SNe can be constructed (Ferrero et al. 2006). The fit equation for the SN component has the form

$$F_\nu^{\rm SN}\left(x = \frac{t}{s}\right) = q_1\,\exp\left\{-\left(\frac{(x-q_2)^2}{q_3}\right)\right\}\,x^{q_4} + q_5\,x^{q_6}\,e^{-q_7\,x}, \quad (2)$$

where the first term models the SN rise and peak and the second term the exponential decay. The coefficients q_1–q_7 are determined based on a fit to the numerical SN 1998bw light curves shifted to the redshift under consideration as described in detail in Zeh et al. (2004).

Practically, at first we shift the SN template to the redshift under consideration (including the cosmological k-corrections). Then we approximate this SN light curve by Eq. (2) and finally include it in the numerical fit (Eq. (1)). When shifting the template light curves to a certain redshift, we have to integrate over the filter under consideration. In doing so we take into account that the (k, s) values are different from band to band. In order to take this wavelength dependence into account, we build a sample of monochromatic (k, s) values by interpolating between the corresponding broad-band values of k and s of the template SN. Finally, when performing the light-curve fits (Eq. (1)), the (broad-band) k and s values were allowed to be different from band to band as is the case for SN 1998bw, while the afterglow parameters were not. In other words, afterglows were considered to evolve achromatically.

We always performed a joint fit, that is, we fit all bands simultaneously. To do so we require an achromatic evolution of the afterglow (spectral index β = const.). When fitting the (Galactic extinction-corrected; Schlafly & Finkbeiner 2011) spectral energy distribution (SED) of an afterglow, we assume a power-law shape and in addition allow for a contribution from dust in the GRB host galaxy. In doing so, we use the analytic expressions from Pei (1992) to model extinction light curves based on Small Magellanic Cloud (SMC), Large Magellanic Cloud (LMC), or Milky Way (MW) dust, following Kann et al. (2006). The slope β of the SED of the afterglow is a direct output of the joint fit of the multi-color light curves. When plotting the SED, we refer to the flux density at t = 1 day in case of single power-law fits, and $t = t_{\rm b}$ assuming $n = \infty$ in case of broken power-law fits. In the latter case $t_{\rm b}$ is the break time and n the smoothness of the break. Thereby, $n = \infty$ describes a sharp break (see Zeh et al. 2006 for more details). Similarly, we assume that the break frequency $\nu_{\rm c}$ is either below or above the optical/NIR bands for the entire time span of the data from which the SED was constructed.

Afterglow light curves were fitted following the standard model according to which the observer lies in the cone of a jetted outflow and the observed break time in the optical light curve is a measure for the actual degree of collimation (Rhoads 1999; Sari et al. 1999). Jet half-opening angles are calculated following Frail et al. (2001) for an interstellar medium (ISM) and Bloom et al. (2003) for a wind medium,

$$\Theta_{\rm ISM} = 0.057\left(\frac{2\,t_{\rm b}}{1+z}\right)^{3/8} E_{\rm iso,53}^{-1/8}\left(\frac{\eta}{0.2}\right)^{1/8}\left(\frac{n}{0.1}\right)^{1/8}$$
$$\Theta_{\rm wind} = 0.169\left(\frac{2\,t_{\rm b}}{1+z}\right)^{1/4}\left(\frac{E_{\rm iso,52}}{\eta\,A_\star}\right)^{-1/4}, \quad (3)$$

where Θ is measured in units of radians, n (cm^{-3}) is the gas density, and η is the efficiency of the shock in converting the energy in the ejecta into gamma radiation. The break time $t_{\rm b}$ is measured in days and the isotropic equivalent energy $E_{{\rm iso},x}$ in units of 10^x erg. We assumed $n = 1$ and $\eta = 0.2$. The parameter $A_\star$ describes the wind mass-loss rate. Following Chevalier & Li (2000), we set $A_\star = 1.0$.

2.5. VLT spectroscopy

Spectroscopy with FORS2 mounted at the VLT was performed to reveal the SN features in the case of the two cosmologically nearest events, GRB 120714B and GRB 130831A. In the case of GRB 120714B spectroscopy of the optical transient was performed on the night between Aug 1 and 2, 2012, 18.3 days after the burst (13.2 days in the GRB rest frame; Klose et al. 2012a,b), which was about 2 days (rest frame) after the SN maximum in the r' band (about 3.5–5 days before the peak in the i', z' bands). The exposure time was 4 × 1450 s. Spectroscopy of the optical transient following GRB 130831A was executed with FORS2 on Sep 29 and Sep 30, 2013 (exposure time 2 × 1378 s in each run), 28.5 and 29.5 days after the burst (about 19.5 days in the rest frame; Klose et al. 2013a,b). This was about 6 days (rest frame)

[3] www.swift.ac.uk/swift_portal

Table 1. Summary of the four GRB events studied here.

GRB SN	071112C	111228A	120714B SN 2012eb	130831A SN 2013fu
Redshift z	0.823	0.7163	0.3984	0.4791
T_{90} (s)	15 ± 2	101.2 ± 5.4	159 ± 34	32.5 ± 2.5
$\log E_{\gamma,\mathrm{iso}}$	$52.28^{+0.11}_{-0.12}$	$52.61^{+0.05}_{-0.06}$	$50.76^{+0.12}_{-0.14}$	$51.86^{+0.04}_{-0.04}$
$\log L_{\gamma,\mathrm{iso}}$	$51.10^{+0.15}_{-0.22}$	$50.60^{+0.07}_{-0.09}$	$48.56^{+0.18}_{-0.31}$	$50.35^{+0.07}_{-0.08}$

Notes. Burst durations are given in the observer frame and were taken from http://swift.gsfc.nasa.gov/archive/grb_table/. The isotropic-equivalent energies (in units of erg) were derived from the observed high-energy properties (Briggs & Younes 2011; Golenetskii et al. 2013), and using the statistically inferred high-energy properties of GRBs (Butler et al. 2007). $L_{\gamma,\mathrm{iso}}$ is the time-averaged luminosity (erg s^{-1}) of the burst, here defined as E_{iso}/T_{90}. References for the redshifts are given in Appendix A.

after the SN maximum in the r', i', z' bands. Observations were performed under excellent sky conditions with a mean seeing of 0.″6.

In all observing runs we used the 300V+10 grism, which covers the wavelength range from 4450 to 8650 Å (dispersion 112 Å mm^{-1}, 1.68 Å pixel^{-1} in case of no binning, resolving power $R = 440$ at 5900 Å)[4] together with the GG435 order-sorting filter. Data reduction was performed applying the standard cosmic ray, flatfield, and bias correction using IRAF. Wavelength calibration was performed relative to HgCdHe+Ar calibration lamps. The spectrophotometric standard stars LTT 1020 and LTT 1788 were observed to flux-calibrate the spectra for the SNe associated with GRB 120714B and GRB 130831A, respectively.

In the case of GRB 120714B additional VLT spectroscopy of the optical transient was obtained with X-shooter 0.35 days after the burst (program ID 089.A-0067; PI: J. P. U. Fynbo) and published by Krühler et al. (2015). Data reduction was performed in a standard manner (for details, see Krühler et al. 2015).

3. Results

Here we focus on the phenomenological GRB-SN parameters based on the observed GROND multi-color light curves, that is, the stretch factor s and the luminosity factor k in the different photometric bands. The results of our VLT spectroscopic follow-up campaigns for two of the four GRBs are outlined below. More details on the derived individual afterglow and host-galaxy parameters are provided in the Appendix. Table 1 provides a summary of the properties of the four GRBs studied here.

3.1. Supernova bumps

Following the phenomenological classification scheme as summarized in, for example, Hjorth (2013) and Cano et al. (2017), based on the observed isotropic equivalent luminosity in the gamma-ray band (Table 1), GRB 120714B is an intermediate-luminosity GRB ($48.5 < \log L_{\gamma,\mathrm{iso}} < 49.5$ erg s^{-1}), while the other three are high-luminosity bursts ($\log L_{\gamma,\mathrm{iso}} > 49.5$ erg s^{-1}).

The GROND light curves of the four optical transients (as well as a few host-galaxy magnitudes from other sources and telescopes which were used in the fits) are shown in Fig. 1. These data demonstrate how well GRB-SN light curves can be monitored with 2 m-class optical telescopes even at redshifts beyond $z = 0.5$. In all cases we performed late-epoch observations several hundred to several thousand days after the event in order to obtain a reliable host-galaxy magnitude, which should guarantee a proper subtraction of the host-galaxy flux when the SN fit was performed. Shown in Fig. 1 are only the GROND $g'r'i'z'$ band data since in no case were we able to detect the SN component in JHK_s[5]; successful NIR observations of GRB-SN light curves remain a challenge[6], not to mention the fact that early NIR observations of SN 1998bw do not exist. The best-sampled cases are GRBs 120714B and 130831A, and the error bars of their derived SN light-curve parameters (luminosity factor k, stretch factor s) are correspondingly small (Table C.1).

The light-curve fit revealed that all four SNe were less luminous than the template SN 1998bw ($k < 1$), though in some cases within the 1σ error bar a $k > 1$ in a certain photometric band is not ruled out. Within the statistical uncertainties, only the SN associated with GRB 111228A might have developed slower than SN 1998bw (i.e., $s > 1$); all others developed faster ($s < 1$).

All four events are characterized by a rather small magnitude difference ($\lesssim$1 mag) between the peak of the SN bump (as the sum of SN, afterglow and host-galaxy flux) and the magnitude of the underlying host galaxy. All four events do however notably differ in their magnitude difference between the peak of the emerging SN component and the flux of the optical transient (OT) at $t_{\mathrm{obs}} = 1$ day. The light curve of the OT that followed GRB 111228A was rather typical for GRB SN events at moderate redshifts (see Zeh et al. 2004, 2005b). At early times the afterglow flux clearly dominated the light, while the SN bump was rather modest, with its peak around 2–3 weeks after the burst. In the case of GRB 071112C and GRB 130831A this difference in magnitude at $t_{\mathrm{obs}} = 1$ day was only about 1 mag, while it was even negative for GRB 120714B, indicating for the latter case a relatively low-luminosity afterglow (see also Sect. 4.3). In this respect the light curve of the OT that followed GRB 120714B is phenomenologically closer to nearby GRB SN events such as GRB 031203/SN 2003lw (e.g., Malesani et al. 2004) and GRB/XRF 060218/SN 2006aj (e.g., Ferrero et al. 2006).

What is immediately apparent in the light curves is that only for GRB 130831A do our data reveal an indisputable SN bump in the g' band. In the case of GRB 071112C an inspection of the GROND g'-band light curves seems to suggest the existence of a break around 2 days and as such also a rising SN component. However, when following this ansatz further we encountered some shortcomings with the corresponding fit results (see Appendix A.1). Also, for this event no contemporaneous break is apparent in the X-ray light curve (see the *Swift*/XRT repository, Evans et al. 2007) which one would expect to find if this feature were due to a collimated explosion and if X-ray and optical flux had a common origin. Therefore, also for this burst we focused on a model with no break, which actually provides a better reduced χ^2 for the joint fit than the approach based on a broken power law.

The lack of a clearly detectable SN component in the g' band for GRBs 071112C, 111228A, and 120714B is worth noting. It is probably primarily due to metal-line absorption in the UV bands (e.g., Olivares et al. 2015) and not due to substantial host-galaxy

[4] See the FORS2 User Manual dated 26/02/2013, page 12.

[5] We note that early NIR observations of SN 1998bw do not exist; there is no template for these bands.

[6] E.g., GRB 031203/SN 2003lw (Cobb et al. 2004; Gal-Yam et al. 2004); GRB 060218/SN 2006aj (Cobb et al. 2006; Kocevski et al. 2007); GRB 100316D/SN 2010bh (Olivares et al. 2012); GRB 130702A/SN 2013dx (Toy et al. 2016).

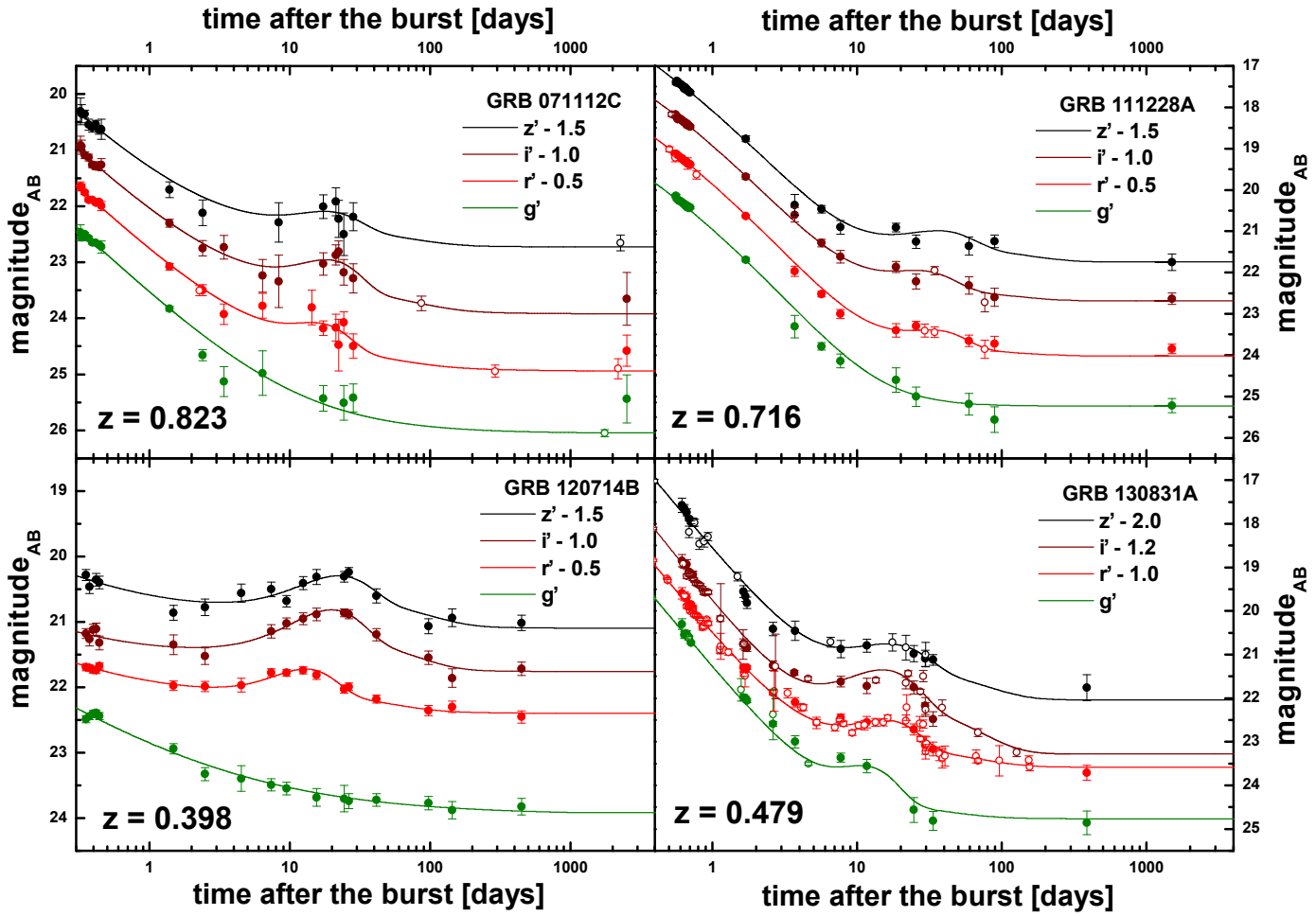

Fig. 1. Afterglow and SN $g'r'i'z'$ light curves of the four SNe in our sample (apparent AB magnitudes are not corrected for Galactic extinction; time refers to the observer frame). Filled circles represent GROND data and open circles represent data taken from the literature. *Top left panel*: the r'-band data point at $t \sim 300$ days was taken from Vergani et al. (2015), other late-time data are listed in Table C.11. *Top right panel*: the light curves include GROND data (Table C.6) as well as late-time data points from the TNG (Table C.11). *Bottom left panel*: for the GROND data see Table C.9. *Bottom right panel*: data points stem from GROND observations (Table C.10) as well as (in $r'i'z'$) from Cano et al. (2014).

visual extinction along the line of sight; the corresponding values we found for $A_V^{\rm host}$ based on the afterglow light curve fits lie between 0 and ~0.15 mag (Appendices A.1–A.3). Possibly, in these three cases the visibility of the SN bump in the g' band is also affected by the comparably bright afterglow and/or underlying host galaxy. Otherwise, for GRB 120714B the VLT spectrum of the accompanying SN shows that the g'-band window is dominated by metal-line absorption, which reduces the flux in this band correspondingly (Fig. 2). Last but not least it has to be taken into account that our light curve fits are based on published *UBVRI* light curves of SN 1998bw (Galama et al. 1998). Consequently, for the given redshifts in particular, our g'-band templates represent an extrapolation into the ultraviolet domain, where in our calculations we assume that the flux density of the SN falls $\propto \nu^{-3}$.

We finally note that with respect to their redshifts GRBs 071112C and 111228A resemble the long GRBs 040924 (z = 0.86) and 041006 (z = 0.71), which also revealed evidence for a SN bump (Stanek et al. 2005; Soderberg et al. 2006). Both SNe were probably dimmed by host-galaxy extinction by 1.5 and 0.3 mag, respectively, but could be observed with HST until about 120 days post-burst (Soderberg et al. 2006). In both cases the SN 1998bw light-curve template fits the observations well.

3.2. Spectroscopic identification of SN light

For two of the four events discussed here (GRBs 120714B and 130831A) additional VLT spectroscopy was obtained that revealed the underlying SNe based on their characteristic broad-band features (now designated SN 2012eb, Klose et al. 2012b, and SN 2013fu, Klose et al. 2013a, respectively)[7]. In addition, the VLT spectroscopy allowed for measurements of the photospheric expansion velocities close to maximum light of the two SNe. Since these spectra are relatively noisy, a boxcar filter was applied in order to recover their overall shape. Depending on the chosen boxcar smoothing parameter, this not only reveals several prominent absorption troughs, but also shows the tight morphological similarity between both SN spectra, even though the corresponding cosmological redshift as well as relativistic Doppler blueshift are different from each other (Fig. 2).

Since for both events no pure host-galaxy spectra could be obtained with the VLT, we use the template spectra that followed from the `Le PHARE` fits (Appendix A) to reveal where prominent emission lines might lie. These are lines due to star-formation

[7] The reduced spectra have been uploaded to the Weizmann Interactive Supernova Data Repository (WISeREP) at https://wiserep.weizmann.ac.il/.

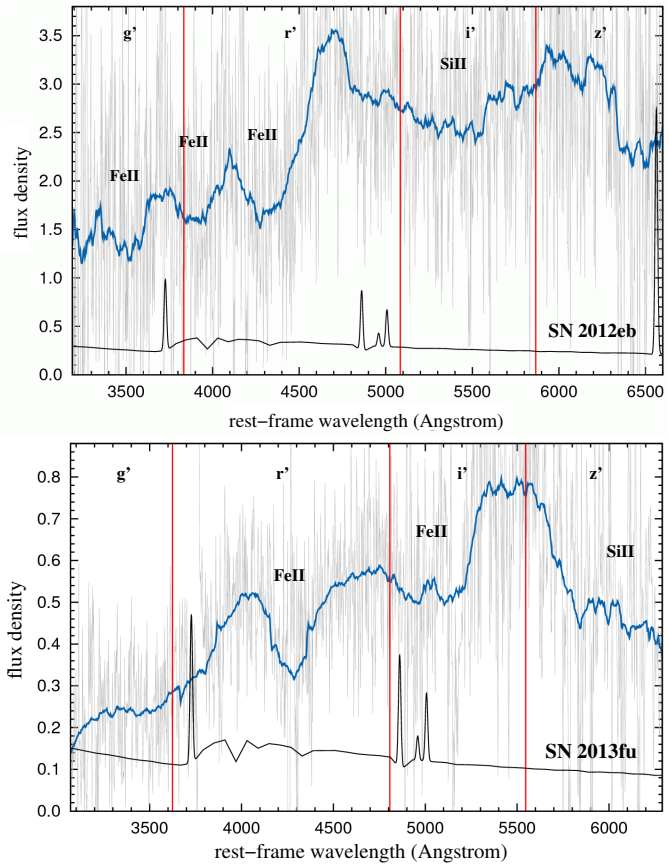

Fig. 2. FORS2 spectra of SN 2012eb and SN 2013fu (plus underlying host-galaxy emission). These spectra are not host-galaxy subtracted, since no spectra of the hosts could be taken. In gray is shown the original spectrum and in blue the spectrum smoothed with a boxcar filter of 250 Å in width. The spectra are shifted into the GRB rest frames but the flux density (in units of 10^{-18} erg s^{-1} cm^{-2} Å^{-1}) is measured in the observer frame. Also drawn are the positions and widths of the GROND filter bands in the GRB rest frame. We note that in the case of the g' and the z' bands the (redshifted) filter width is slightly larger than shown here (Greiner et al. 2007, 2008). *Top panel*: SN 2012eb, taken on day 18.3 post-burst (observer frame), about 2 days (rest frame) after the SN maximum in the r' band (Klose et al. 2012a,b). *Bottom panel*: SN 2013fu, obtained at a mean time of t = 29 days post-burst (observer frame), about 6 days (rest frame) after the SN maximum in the $r'i'z'$ bands (Klose et al. 2013a,b). Also shown are the host-galaxy template SEDs (black lines; Appendices A.3, A.4) mainly to illustrate where emission lines from the hosts might exist. We note that the predicted (modeled) flux in the emission lines has a substantial error, which is not shown here; see text.

activity from the [O II] $\lambda\lambda$3727, 3729 doublet, Hγ (4341 Å), Hβ (4861 Å), [O III] $\lambda\lambda$4959, 5007, and Hα (6563 Å) (Fig. 2). However, none of these lines are detected in our spectra. This non-detection still agrees with the calculated star-formation rates (SFRs) if the corresponding 1σ error bars are taken into account (Table C.5). Providing confident upper limits on the SFRs via the non-detections of the emission lines in the spectrum is a challenge as the spectra are very noisy. Though, we can exclude 3σ deviations from the model templates in the positive direction.

In the case of SN 2012eb the most prominent absorption trough is located at 5500 ± 100 Å rest frame[8]. The shape

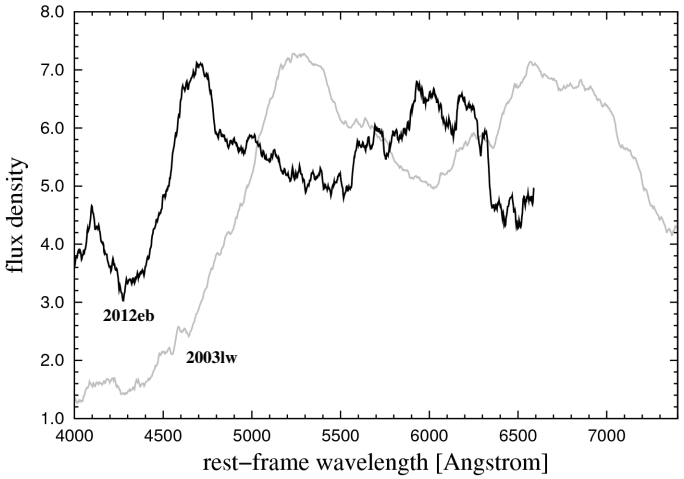

Fig. 3. Comparison of the spectrum of SN 2003lw taken on Dec 20, 2003, ∼15 days (rest frame) after the burst and ∼3 days before the SN maximum in the R_c band (in light gray, Malesani et al. 2004) with the spectrum of SN 2012eb taken between Aug 1 and 2, 2012, 13.2 days after the burst (black line; shifted to the rest frames). The spectrum of SN 2003lw was taken from the *Open Supernova Catalog* data base (Guillochon et al. 2017). According to Mazzali et al. (2006), this implies that on Dec 20 the expansion velocity was 17 000 ± 1000 km s^{-1}. The SN 2012eb spectrum shows a substantially higher blueshift. Both spectra are smoothed with a boxcar filter of 250 Å width. Flux densities are arbitrarily scaled.

of this feature is very much reminiscent of the one seen in SN 2003lw/GRB 031203 (z = 0.1055) around maximum light (Fig. 3). It is generally attributed to Si II λ 6355, while the broad absorption features bluewards of Si II are believed to be due to blended lines of single-ionized iron (Nakamura et al. 2001; Malesani et al. 2004; Mazzali et al. 2006, 2013)[9].

Interpreted in this way, the Si II feature corresponds to a blueshifted velocity of 43 000 ± 5300 km s^{-1}. This means that the large error is a direct consequence of the aforementioned boxcar filtering procedure and the related uncertainty (±100 Å) of the central wavelength of the absorption trough. Applying the SYNOW code (Fisher et al. 1997) to an individual smoothed spectrum provided smaller errors. It also attributed the absorption trough at around 4300 Å to broadened lines of single-ionized Fe $\lambda\lambda$5100 at basically the same high expansion velocity, while the identification of the other broad-band features is less secure.

In the case of SN 2013fu, the spectrum is relatively noisy. The prominent absorption trough redwards of 5500 Å (rest frame) is probably again due to Si II. This feature is partly redshifted out of our spectral window, however; the location of its central wavelength cannot be determined. The shape of the absorption trough centered at around 5000 Å appears to be affected by emission lines from the underlying host galaxy, and therefore it might not be a reliable tracer of the expansion velocity. If the absorption feature centered at 4270 ± 50 Å (rest frame) is due to (dominated by) Fe II λ4570, then the expansion velocity is 20 400 ± 3500 km s^{-1} (Fig. 2).

Compared to other GRB SNe where the photospheric expansion velocity was measured via the Si II λ6355 or the Fe II feature(s) the inferred velocity for SN 2012eb is the highest so far measured close to the time of maximum light (e.g.,

[8] The relatively large error has its origin in the application of the boxcar filtering procedure to the spectra. Depending on the chosen boxcar smoothing parameter (number of pixels), the shape and position (wavelength) of the broad-band absorption feature varies.

[9] Si II λ6355: doublet $\lambda\lambda$6347, 6371; Fe II λ4100: multiple blends; Fe II λ4570: potentially blended lines of Mg II λ4481, He I λ4471, Ti II λ4550; Fe II λ5100: triplet $\lambda\lambda$4924, 5018, 5169.

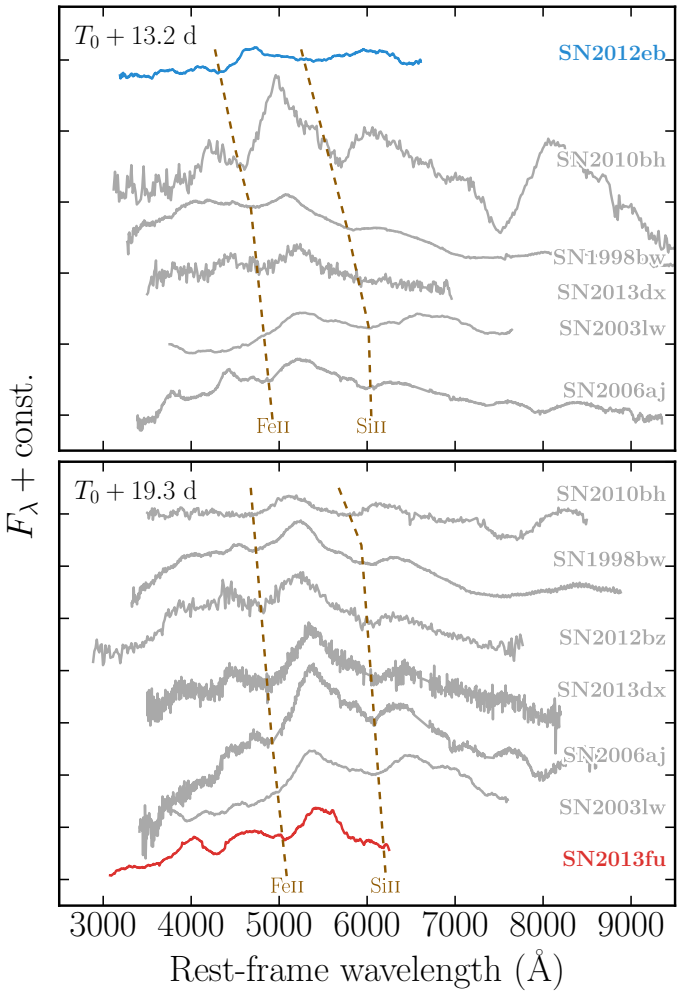

Fig. 4. Comparison of SNe 2012eb (blue) and 2013fu (red) to spectra of other GRB SNe (gray) at two different phases, 13.2 and 19.3 days past explosion, respectively. All comparisons are made in the rest frame. The dashed lines connect the approximate minima for the FeII and SiII features, and the spectra are shown in an expansion velocity sequence from the fastest (SN 2010bh) to the slowest (SN 2006aj). All data are corrected for Galactic extinction along the line of sight. Data references: SN 1998bw: Patat et al. (2001), SN 2003lw: Malesani et al. (2004), SN 2006aj: Pian et al. (2006), SN 2010bh: Bufano et al. (2012), SN 2013dx: D'Elia et al. (2015), SN 2012bz: Schulze et al. (2014). Further data were taken from the Interactive Supernova data REPository (WISeREP; Yaron & Gal-Yam 2012). All spectra were corrected for host reddening, except for that of SN 2003lw.

Ben-Ami et al. 2012; Schulze et al. 2014; Olivares et al. 2015; Cano et al. 2017). Even higher velocities though, close to 50 000 km s^{-1}, have been reported for GRB 100316D/SN 2010bh during the SN rise time (Bufano et al. 2012). On the other hand, SN 2013fu lies rather at the lower end of the expansion velocities for GRB SNe close to maximum light and measured via the Fe II features (Figs. 4, 5).

Last but not least it is worth stressing that the isotropic equivalent energy of GRB 120714B in the gamma-ray band (Table 1) was more than 1000 times less than the isotropic equivalent energy of GRB 130427A/SN 2013cq at $z = 0.34$ (log $E_{\rm iso}$ [erg] = 53.98; Xu et al. 2013) and ten times higher than that of GRB 100316D/SN 2010bh at $z = 0.059$ (log $E_{\rm iso}$ [erg] = 49.6; Starling et al. 2011); the corresponding SN explosion as well as light-curve parameters however are not substantially different from each other (see also Melandri et al. 2014).

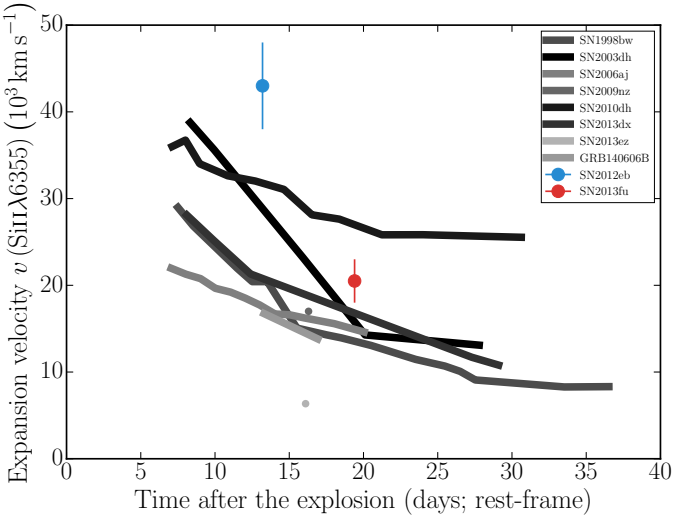

Fig. 5. Evolution of the expansion velocities measured from SiIIλ6355 for SN 2012eb and SN 2013fu and a comparison sample (for references see Fig. 4) of GRB SNe with good spectroscopic data.

3.3. Excess of blue light in the optical transient that followed GRB 120714B

During the GROND first-epoch observations of the optical transient that followed GRB 120714B, at $t_{\rm obs} = 0.265$ days, the seeing was about 3″, resulting in a relatively large magnitude error in i' and z' (Table C.9). Therefore, we analyzed the early SED of the optical transient (all data are corrected for Galactic reddening along the line of sight; $E^{\rm Gal}_{(B-V)} = 0.01$ mag; Schlafly & Finkbeiner 2011) based on the GROND data taken at $t_{\rm obs} = 0.354$ days in combination with the VLT/X-shooter spectrum taken at basically the same time (at $t_{\rm obs} = 0.353$ days post burst; Fig. 6). After subtracting the (smoothed) broad-band SED of the underlying host-galaxy flux (based on the `Le PHARE` fit; Appendix A.3), an inspection of the X-shooter data shows that bluewards of ~600 nm the flux density is increasing with increasing frequency ($(r' - g') > 0.5$ mag). This is opposite to what is expected for the SED of a GRB afterglow. This excess of blue light can be modeled as the low-energy tail of soft thermal X-ray emission, similar to what was observed in other low-redshift GRB SNe (GRB/XRF 060218/SN 2006aj, Campana et al. 2006; GRB/XRF 100316D/SN 2010bh, Cano et al. 2011; Olivares et al. 2012; GRB 120422A/SN 2012bz, Schulze et al. 2014)[10].

Support for the interpretation of the excess of blue light as an underlying additional black-body component comes from the spectral slope in the wavelength range between about $\lambda_{\rm rest} = 320$ nm and 450 nm. Here, the host-subtracted SED can be fit with a power law and the best-fit spectral slope ($\beta = -1.78 \pm 0.19$) lies close to the value expected for the Rayleigh-Jeans tail of a black body ($\beta = -2$). For the given wavelength region this requires a temperature $T^{\rm rest}_{\rm bb} \gtrsim 10$ eV (rest frame).

Since the first discovery of a thermal component in the afterglow of GRB/XRF 060218/SN 2006aj (Campana et al. 2006), the preferred interpretation in the literature is that this is emission from the cooling photosphere after SN shock breakout (Waxman et al. 2007; Nakar & Sari 2010; but see also Irwin & Chevalier 2016; Ruffini et al. 2017). Substantial

[10] In the case of GRB 120422A/SN 2012bz the black-body component had a low luminosity compared to the afterglow and a temperature that was too low to show up in the X-ray band.

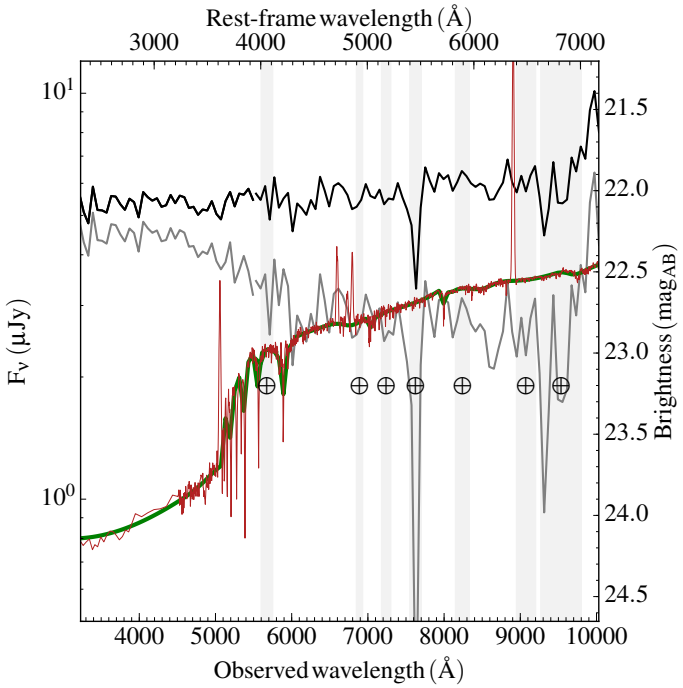

Fig. 6. VLT/X-shooter spectrum of the optical transient that followed GRB 120714B, taken at t_{obs} = 0.353 days after the burst. The binned original spectrum is shown in black, the host-galaxy SED template as obtained from the `Le PHARE` fit (Appendix A.3) in red. The green curve shows the smoothed host-galaxy template that was subtracted from the original spectrum. The host-subtracted SED is drawn in light gray. Flux densities refer to the observer frame. Telluric features are indicated.

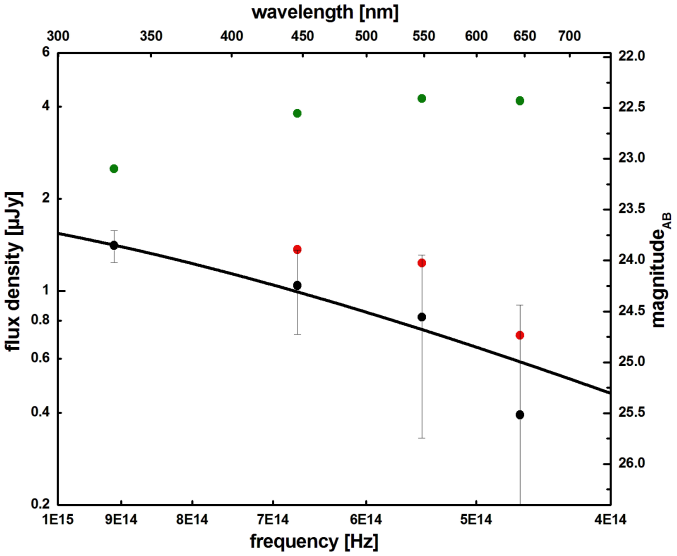

Fig. 7. Rest-frame SED of the optical transient following GRB 120714B at t_{obs} = 1.48 days based on the GROND $g'r'i'z'$-band data (Table C.9). Green-colored data points refer to observed, red-colored to host-subtracted, and black-colored to (host+SN)-subtracted magnitudes. The thick black line shows the best fit: the SED of a black body with T_{bb}^{rest} = 2.4 ± 0.7 eV. The data imply that the peak of the black-body flux still lies bluewards of the g' band. Wavelengths and frequencies are given in the host-galaxy frame.

observational efforts have been put forward to search for such a signal in the X-ray data of long-duration GRBs (e.g., Olivares et al. 2012; Starling et al. 2012; Sparre & Starling 2012) as well as in the optical data of SNe in general (e.g., Förster et al. 2016), mostly with negative results. As such, adding another positive detection to the database would be of great interest.

The lack of X-ray data does not allow us to determine T_{bb}^{rest} at t_{obs} = 0.353 days in a more precise way. However, we can estimate its value by taking into account the optical GROND multi-color data at t_{obs} = 1.48 days. At that time the emerging SN component cannot be neglected anymore. After the subtraction of host and SN light, the $(r'-g')$ color is still positive (+0.3 mag), corresponding to a spectral slope of $\beta \sim -1$. Compared to the first-epoch observations the SED has clearly flattened. A fit of our host- and SN-subtracted (host-frame) data with a black-body component now yields T_{bb}^{rest} = 2.4 ± 0.7 eV, which we adopt as a lower limit for T_{bb}^{rest} at 1.48 days (observer frame; Fig. 7). Smaller temperatures are excluded as they would change the shape of the SED in a way that causes the data to become incompatible with the model. Higher temperatures are formally not constrained as the spectral slope would be at most $\beta = -2$, which is qualitatively still compatible with the observed blue color. If we adopt the hypothesis that we see radiation from a cooling black body, then the lower bound on T_{bb}^{rest} implies that at 1.48 days the peak of the black-body component had not yet passed the g' band.

The lower limit we can place on T_{bb}^{rest} at t_{obs} = 1.48 (in the following t_2) days can now be used to constrain its value at t_{obs} = 0.353 days (in the following t_1). Following the procedure outlined in Olivares et al. (2012), for the time evolution of T_{bb} we make the ansatz $T(t) = T_{init} - a\,t^b$, where T_{init}, a, and b are constants. Consequently, for two different times $T(t_1) - T(t_2) = a\,(t_2^b - t_1^b)$, where we measure T in keV and t in seconds (in the host frame). Using $T_{bb}^{rest}(t_2 = 1.48\,\text{days}) = 2$ eV, a = 0.0036 and b = 0.3 ± 0.2 (as was found by Olivares et al. 2012 for GRB/XRF 100316D/SN 2010bh), we obtain $T_{bb}^{rest}(t_1 = 0.353\,\text{days}) \gtrsim 40$ eV. Similar results are obtained when we use the parameters that describe the temperature evolution of GRB/XRF 060218/SN 2006aj (Campana et al. 2006). Using the data of these latter authors, we find a = 0.0006, b = 0.47 and obtain $T_{bb}^{rest}(t_1 = 0.353\,\text{days}) \sim 65$ eV.

In principle, a cooling black body should progressively shift the peak flux of the thermal emission redwards into the optical bands, potentially leading to a detectable time evolution of the observed broad-band optical/NIR SED, and perhaps even a rebrightening, as was observed for GRB/XRF 060218/SN 2006aj (Campana et al. 2006). Unfortunately, for GRB 120714B/SN 2012eb the rapid rise of the SN component in the $r'i'z'$ bands prevents any detection of such an effect at later times.

Once the black-body component has been identified in the host-subtracted data we can derive the spectral slope of the pure afterglow light at t_{obs} = 0.353 days. In doing so, the scatter of the X-shooter data at larger wavelengths and the uncertainty of the J-band magnitude do not constrain the spectral slope β tightly enough; adopting T_{bb}^{rest} = 50 eV for the black-body component, the best fit to the $g'r'i'z'J$-band data provides β = 0.7 ± 0.4 (Fig. 8). We note that in this figure all data are corrected for host-galaxy flux. Here, the $g'r'i'z'$-band data points are based on GROND observations of the transient at t_{obs} = 0.354 days. The J-band data point, however, is based on GROND observations at t_{obs} = 0.396 days since the transient was not detected in this band at earlier times (Table C.9). Therefore, this data point was shifted to t_{obs} = 0.353 days before the host-galaxy flux was subtracted. In doing so, we assumed a time evolution of the J-band flux according to a power law with α = 0.58, as follows from our light-curve fits (Sect. 3.1; Table C.2). This procedure is justified since the data suggest that around 0.35–0.40 days the

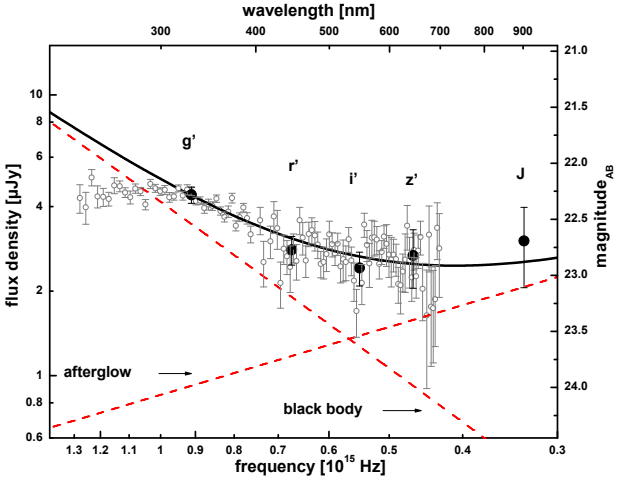

Fig. 8. Host-subtracted SED of the optical transient following GRB 120714B at $t = 0.353$ days (observer frame), consisting of GROND (black) and binned X-shooter (gray) data (step size 60 nm). The thick black line shows the best fit for a two-component model (indicated by the red broken lines) consisting of afterglow light with a spectral slope of $\beta = 0.7$ and a black body with a temperature of $T_{\rm bb}^{\rm rest} = 50$ eV. Wavelengths and frequencies are given in the host-galaxy frame.

host-galaxy corrected flux in the J band was dominated by afterglow light.

We finally note that bluewards of the g' band the flux density of the host-subtracted SED clearly deviates from a combined black body and afterglow fit, and there is a lack of flux with increasing frequency (Fig. 8). Milky Way-like dust along the line of sight with $A_V^{\rm host} \sim 0.5$ mag could explain this feature. The deduced SN peak luminosities (parameter k; Table C.1) would then scale correspondingly, which could potentially also explain the non-detection of the SN in the g' band. However, we cannot rule out that this feature is (at least partly) an artifact introduced by the subtraction of the host-galaxy synthetic spectrum (green curve in Fig. 6), which is not well known bluewards of the g' band. Therefore, we followed Occam's razor and adopted for this burst $A_V^{\rm host} = 0$ mag.

4. Discussion

4.1. Bolometric SN light curves

In order to compare our sample of GRB SNe with the current data base of GRB SNe, we need to construct bolometric light curves. In doing so, we are confronted with the problem that these targets are at moderate redshifts. Even if there is a good set of multi-color data in the observer frame, in the SN rest frame the situation can look much less favorable. For instance, for the cases discussed here we lack any GRB-SN detection redwards of the z' band. In the worst case (GRB 071112C; $z = 0.823$) the z' band is centered at 490 nm rest-frame wavelength, in the best case (GRB 120714B, $z = 0.398$) at 639 nm.

To correct for, for example, the unknown NIR part of a SN SED, it is usually assumed that the SED can be reconstructed based on its snapshot in the optical bands (e.g., Tomita et al. 2006; Takaki et al. 2013; Olivares et al. 2015). We follow this approach in a more rigorous way by adopting the following two assumptions: (i) The bolometric light curve of a GRB SN can be described by a stretch and a luminosity factor as well, and these two factors can be normalized to the bolometric light curve of SN 1998bw. (ii) The bolometric stretch and luminosity factor (in the following $s_{\rm bol}$ and $k_{\rm bol}$) can be constructed from the stretch and luminosity factors in the optical/NIR bands. In other words, we assume that the in-some-way wavelength-averaged SN light curve parameters in the optical bands are a very good proxy for the bolometric light-curve parameters (light-curve shape). In order to avoid the introduction of too many mathematical symbols, and in order to underline that the procedure which follows relies on the aforementioned basic ideas, in the following we always refer to $s_{\rm bol}$ and $k_{\rm bol}$; though the reader should keep in mind that these calculated numbers are approximate (quasi-bolometric) values for the true (and basically unknown) numbers of $s_{\rm bol}$ and $k_{\rm bol}$.

In doing so, we define a quasi-bolometric light-curve parameter $k_{\rm bol}$ as

$$k_{\rm bol} = \left(\frac{1}{n} \sum_{i=1}^{n} k_i^3 \right)^{1/3} . \quad (4)$$

We include in Eq. (4) the $r'i'z'$ bands, but do not use the g' band, that is, we have $n = 3$.[11]

Our omission of the g' band is immediately justified by the non-detection of the GRB SNe in g' in three of the four cases discussed here. For SN 1998bw it is $k_i = 1$ for all i so that Eq. (4) delivers $k_{\rm bol} = 1$, whatever i (photometric bands) are selected.

Similar to Eq. (4), we define a quasi-bolometric stretch factor

$$s_{\rm bol} = \left(\frac{1}{n} \sum_{i=1}^{n} s_i^3 \right)^{1/3} . \quad (5)$$

It should be stressed that there is *ad hoc* no physical reason for the use of a cubic averaging of the light-curve parameters. Also, the obvious weakness of our definition of $k_{\rm bol}$ is that it ignores any redshift effect. For different SNe at different redshifts the corresponding k_i-parameters are measured in the observer frame and hence in the SNe host frames they can trace different wavelength regimes. As such we caution that we build the quasi-bolometric light curve based on snapshots of the light curves in different parts of a supernova SED. We adopt here the assumption that $k_{\rm bol}$ closely follows a weighted ensemble average of the k_i values. Our way of averaging gives photometric bands with a large k factor a higher weight than bands with a smaller k factor. The philosophy behind this approach is that it is probably more likely to underestimate the flux in a certain band (potentially affected by unknown absorption) than to overestimate it. Clearly, this argument cannot be applied to the averaging of the s_i values. Nevertheless, here we use the same kind of averaging again in order to achieve some "internal mathematical consistency" in our approach. Much more justified equations to construct quasi-bolometric parameters might be found, but for the present discussion this is not strongly relevant.

For further discussion we need the SN expansion velocities during maximum light, $v_{\rm ph;peak}$. To determine this, we follow Sanders et al. (2012) and make the ansatz

$$v_{\rm ph}(t) = v_{\rm ph;peak} \left(\frac{t}{t_{\rm peak}} \right)^{-\alpha} . \quad (6)$$

In addition, we define $t_{\rm peak,bol} = s_{\rm bol} \times t_{\rm peak,bol,bw}$. Based on the analysis of Sanders et al. (2012) we assume $\alpha = 0.8 \pm 0.2$ for GRB SNe.

In the case of GRB 120714B/SN 2012eb the bolometric peak time was at $t_{\rm peak,bol} = 13.6 \pm 0.7$ days (rest frame; Table C.1),

[11] In order to be consistent, also in the case of GRB 130831A we did not use the k value for the g' band (Table C.1).

Table 2. Bolometric (k, s) values and redshifts for 17 GRB SNe.

GRB	SN	$k_{\rm bol}$	$s_{\rm bol}$	z
990712		0.68 ± 0.11	0.67 ± 0.05	0.433
020405		0.76 ± 0.09	0.85 ± 0.05	0.691
030329	2003dh	1.46 ± 0.16	0.87 ± 0.01	0.1685
031203	2003lw	1.47 ± 0.26	1.08 ± 0.15	0.1055
071112C		0.60 ± 0.10	0.75 ± 0.15	0.823
080319B		1.03 ± 0.10	0.80 ± 0.05	0.938
081007	2008hw	0.93 ± 0.09	1.03 ± 0.06	0.530
091127	2009nz	1.30 ± 0.15	0.97 ± 0.04	0.490
100316D	2010bh	0.48 ± 0.01	0.62 ± 0.01	0.0591
101219B	2010ma	1.41 ± 0.09	0.76 ± 0.06	0.552
111209A	2011kl	2.41 ± 0.16	1.10 ± 0.03	0.677
111228A		0.75 ± 0.13	1.43 ± 0.14	0.716
120422A	2012bz	1.13 ± 0.01	0.91 ± 0.01	0.283
120714B	2012eb	0.69 ± 0.04	0.86 ± 0.04	0.3984
130702A	2013dx	1.27 ± 0.03	0.86 ± 0.01	0.145
130831A	2013fu	0.77 ± 0.04	0.75 ± 0.02	0.4791
140606B		0.70 ± 0.02	0.96 ± 0.06	0.384

Notes. For the first four events the $k_{\rm bol}, s_{\rm bol}$ values are based on VR_cI_c-band data. For all other SNe these values are based on $r'i'z'$-band data. The four GRB SNe discussed here are highlighted. Bolometric values were calculated using Eqs. (4) and (5).

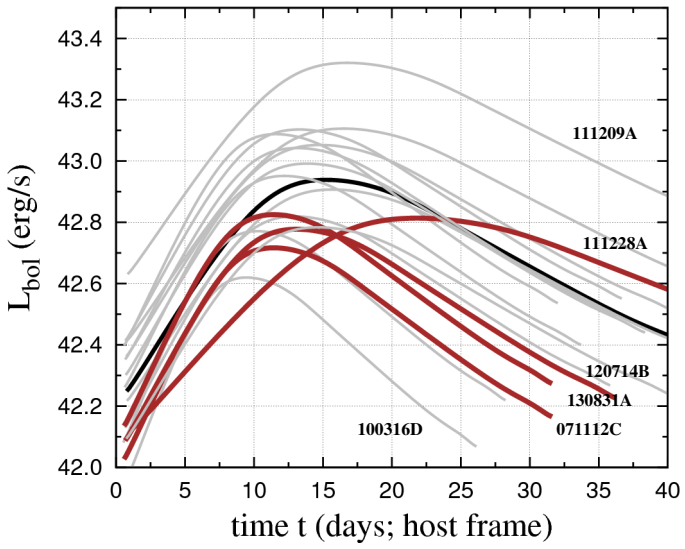

Fig. 9. Bolometric luminosity of the 17 GRB SNe according to Table 2. In addition we show the bolometric light curve of SN 1998bw (in black), which we took from Greiner et al. (2015; their Fig. 3) and performed a smoothed spline fit. All other SN light curves were then scaled accordingly using the corresponding bolometric values for the stretch and luminosity factor (Eq. (1)). The four GRB SNe discussed here are drawn in brown. We note that this plot is a visualization of the $(s_{\rm bol}, k_{\rm bol})$ values in Table 2 and is not based on individual data points.

while the SN spectrum was taken at $t = 13.2$ days (rest frame). Using Eq. (6), we obtain $v_{\rm ph;peak} = 42\,000 \pm 5500\,{\rm km\,s^{-1}}$. In the case of GRB 130831A/SN 2013fu, we have $t_{\rm peak,bol} = 11.9 \pm 0.3$ days (Table C.1), while the SN spectrum was taken at $t = 19.5$ days. This leads to $v_{\rm ph;peak} = 30\,300 \pm 6000\,{\rm km\,s^{-1}}$.

In order to construct a comparison sample, we used the homogeneous multi-color data set of (s, k) pairs published by Kann et al. (2016) for GRB SNe from the years between 1999 and 2014 and applied Eqs. (4) and (5). In addition, we included the GROND multi-color fit results for GRB 101219B/SN 2010ma (Olivares et al. 2015). Finally, we selected only GRB SNe with known (k, s) data in the $r'i'z'$ or VR_cI_c bands. Altogether the entire sample contains 17 events, including the four GRB SNe studied here (but excluding the template GRB 980425/SN 1998bw; Table 2).

What is apparent in the data is that low- and medium-z GRB SNe favor the case $s_{\rm bol} < 1$. Only four events have $s_{\rm bol} > 1$ (neglecting the error bars). The spread in the individual $k_{\rm bol}$ factors is much larger, nine events have $k_{\rm bol} < 1.0$ and eight have $k_{\rm bol} > 1.0$. This might reflect the fact that the determination of $k_{\rm bol}$ depends on the (adopted) host-galaxy extinction along the line of sight as well as the (adopted) internal SED of the corresponding SN while the determination of $s_{\rm bol}$ does not. It is worth mentioning that there is no evidence for a redshift-dependence of these parameters.

The $k_{\rm bol}, s_{\rm bol}$ pairs were then used to calculate bolometric light curves by using the corresponding light curve of SN 1998bw as a reference (Greiner et al. 2015; Fig. 9).

What is immediately apparent in Table 2 is the outstanding large stretch factor we have found here for the SN associated with GRB 111228A. This solution has to be taken with care, however. As we have noted in Appendix A.2, due to the rather weak SN bump in this case the fit is rather sensitive to the deduced afterglow parameters. For example, fitting the *Swift*/XRT light curve from 2000 s onwards, and regardless of whether we include the last X-ray data point in the fit or not, the post-break decay slope is much shallower than implied by the GROND data, closer to 1.4. Consequently, the reported 1σ error for this stretch factor might therefore be even larger than given in Table 2.

Neglecting this burst as an outlier, for GRB SNe the observed $s_{\rm bol}, k_{\rm bol}$ pairs suggest that a large $s_{\rm bol}$ implies a large $k_{\rm bol}$ (Fig. 10; see also Cano 2013, 2014; Cano et al. 2017). The data can formally be fitted with a function $k_{\rm bol} \sim s_{\rm bol}^a$, a = const., but the scatter in the data is large and the result of the fit (i.e., the fit parameter a) sensitive to the exclusion of individual events. While hidden systematic errors could affect our determination of the individual $k_{\rm bol}$ and $s_{\rm bol}$ values, this scatter could also indicate that additional parameters come into play that are not considered in this plot (Klose 2017).

4.2. Supernova explosion parameters

We used the Arnett model for type-Ia SNe (Arnett 1982), its slight modification by Valenti et al. (2008)[12], and the *Stritzinger–Leibundgut relation* (Stritzinger & Leibundgut 2005)[13] to derive the explosion parameters (released mass of radioactive nickel $M_{\rm Ni}$, ejected mass $M_{\rm ej}$, kinetic energy of the ejecta $E_{\rm kin}$). In doing so, we normalize all values to SN 1998bw. As such we are insensitive to slight disagreements in the literature about the corresponding absolute values for SN 1998bw (e.g., the discussion in Dessart et al. 2017). Within this context we have (Klose 2017):

$$M_{\rm Ni;\,norm} = k_{\rm bol}\,\frac{\eta(t_{\rm peak}^{\rm bw})}{\eta(t_{\rm peak})}, \quad \text{with} \tag{7}$$

$$\eta = 6.45\,{\rm e}^{-t_{\rm peak}/8.76} + 1.45\,{\rm e}^{-t_{\rm peak}/111.27}, \tag{8}$$

[12] For applications and explanations of the Arnett–Valenti equations see, e.g., Olivares et al. (2015), Wheeler et al. (2015), Toy et al. (2016).
[13] See, e.g., Takaki et al. (2013) and Prentice et al. (2016).

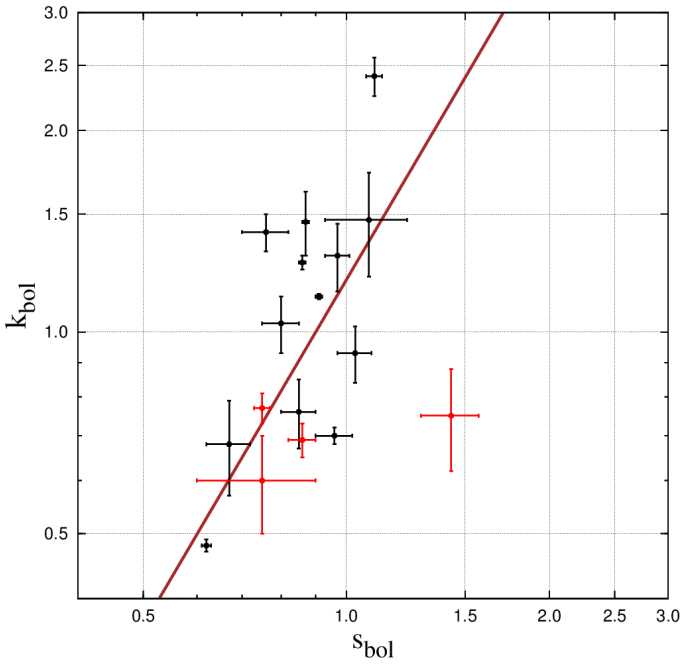

Fig. 10. Bolometric luminosity $k_{\rm bol}$ vs. bolometric stretch factor $s_{\rm bol}$ for the 17 GRB SNe listed in Table 2. Red-colored data points refer to the four GRB SNe discussed here, black-colored data points to the remaining 13 events. We note that SN 1998bw is not included here (by definition, $s^{\rm bw}_{\rm bol} = 1, k^{\rm bw}_{\rm bol} = 1$). The best fit is shown for an ansatz $k_{\rm bol} \sim s^{a}_{\rm bol}$, $a = 1.7$ (excluding in the fit GRBs 111209A, 111228A and SN 1998bw).

$$\left(\frac{M^3_{\rm ej}}{E_{\rm kin}}\right)_{\rm norm} = s^4_{\rm bol}\left(\frac{\kappa^{\rm bw}}{\kappa}\right)^2, \quad (9)$$

where $t_{\rm peak}$ is the peak time of the SN measured in days and κ is the volume and time-averaged matter opacity in the ejecta.

Dessart et al. (2016) have pointed out that the Arnett rule and its underlying model assumptions are well established for type-Ia SNe, but when compared with numerical models for type-II/Ib/Ic SNe the Arnett rule overestimates the amount of released nickel mass by as much as 50%. Moreover, when asymmetric explosions are considered, the derived explosion parameters can change notably (Dessart et al. 2017). We do not consider these issues further but leave the reader with the warning that, in the following, error bars on deduced SN parameters are basically simply mathematical in nature.

Using the *Stritzinger–Leibundgut relation*, in our sample, 8 of the 17 GRB SNe have $k_{\rm bol} > 1$ (neglecting the 1σ error bars); they produced more nickel than SN 1998bw (Fig. 11)[14]. The ratio $M_{\rm Ni}/M^{\rm bw}_{\rm Ni}$ varies between about 0.3 and 2.6. It is highest for GRB 111209A/SN 2011kl (in agreement with Kann et al. 2016; assuming the light curve was powered by ^{56}Ni) and lowest for GRB 990712 and GRB/XRF 100316D/SN 2010bh. Excluding the apparent outlier GRB 111209A, the vast majority (15) of the remaining 16 SNe lie in a relatively narrow range between $M_{\rm Ni}/M^{\rm bw}_{\rm Ni} = 0.56$ and 1.23. Three of the four GRB SNe discussed here (GRB 071112C, 120714B, 130831A) occupy the lower part of this distribution; they produced a rather small amount of radioactive nickel.

[14] This picture does not change when we use the *Arnett–Valenti relation* (Valenti et al. 2008), even though the sample of SNe that falls into this category is now slightly different.

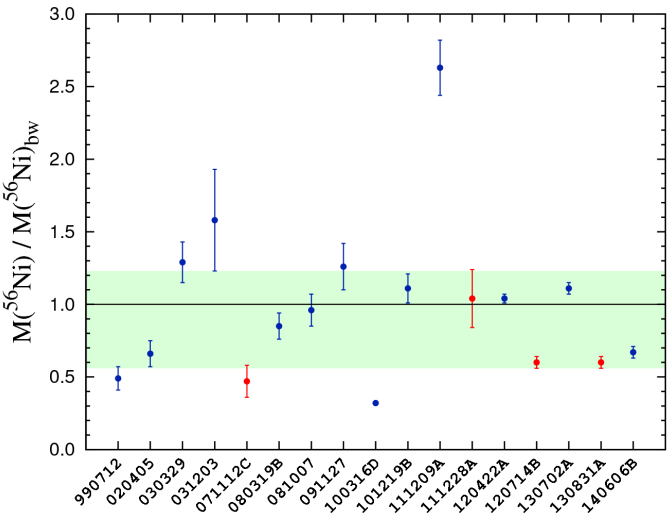

Fig. 11. Ejected mass of ^{56}Ni for the 17 GRB SNe listed in Table 2 according to the *Stritzinger–Leibundgut relation*. In red are shown the results for the four GRB SNe discussed here. Excluding the apparent outlier GRB 111209A, the vast majority (15 SNe) of the remaining 16 SNe lie in the colored region (within their 1σ errors). The black horizontal line highlights the position of the template SN 1998bw.

The ultra-long GRB 111209A/SN 2011kl deserves a special note (Greiner et al. 2015; Kann et al. 2016; Mazzali et al. 2016) as it is an obvious outlier in the distribution ($M_{\rm Ni}/M^{\rm bw}_{\rm Ni} \sim 2.6$). We note however, if $M^{\rm bw}_{\rm Ni} = 0.4\,M_\odot$ (Nakamura et al. 2001) then the absolute value we derive here is in agreement with the one reported in Greiner et al. (2015). It has already been stated by these authors that for SN 2011kl an additional energy source, most likely a newly formed magnetar, might have substantially affected its high peak luminosity (see also Kann et al. 2018). Consequently, the approach we have used here overestimates the amount of released radioactive ^{56}Ni.

Figure 12 shows the ratio $M^3_{\rm ej}/E_{\rm kin}$ for each SN, normalized to SN 1998bw (assuming $\kappa = \kappa^{\rm bw}$). Since this ratio does not depend on the photospheric expansion velocity, it is more reliable than the value for its individual components $M_{\rm ej}$ and $E_{\rm kin}$. Not plotted in Fig. 12 is GRB 111228A since due to the relatively large stretch factor for this SN $(M^3_{\rm ej}/E_{\rm kin})_{\rm norm} = 6.3 \pm 1.6$, which exceeds the parameter space occupied by the other 16 GRB SNe substantially. As noted beforehand, for this event the SN bump is relatively weak and the result of the fit relatively sensitive to the inclusion of individual data points. In other words, the error for $s_{\rm bol}$ is probably larger than what is quoted in Table 2. Neglecting GRB 111228A as an outlier and taking into account the 1σ error bars, the vast majority of all SNe (15 SNe) lie between $(M^3_{\rm ej}/E_{\rm kin})_{\rm norm} = 0.23$ and 1.45.

A calculation of the ejected mass $M_{\rm ej}$ and the kinetic energy $E_{\rm kin}$ in the SN shell requires knowledge of the photospheric expansion velocity $v_{\rm ph}$. In our study, a snapshot of $v_{\rm ph}$ has been obtained only for GRB 120714B/SN 2012eb and 130831A/SN 2013fu. Given that $v_{\rm ph}$ is a function of time and given that its value usually depends on the spectral feature used to measure it (e.g., Cano et al. 2017, their Fig. 6), conclusions on $M_{\rm ej}$ and $E_{\rm kin}$ are less secure even if we are normalizing our results to the corresponding parameters of SN 1998bw.

Using $v_{\rm ph;peak} = 42\,000 \pm 5500\,{\rm km\,s^{-1}}$ for SN 2012eb, we obtain $M_{\rm ej}/M^{\rm bw}_{\rm ej} = 2.2 \pm 0.5$ for the ejected mass and a kinetic energy of $E_{\rm kin}/E^{\rm bw}_{\rm kin} = 20.0 \pm 11.1$. For SN 2013fu

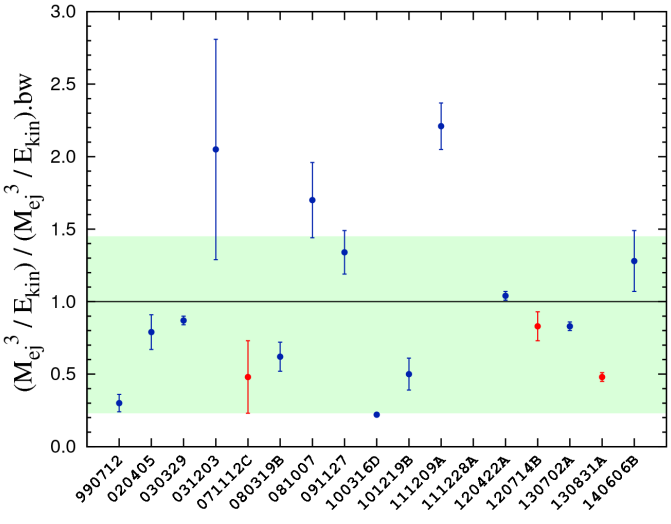

Fig. 12. Ratio M_{ej}^3/E_{kin} for the SNe listed in Table 2 normalized to the corresponding value of SN 1998bw and adopting $\kappa = \kappa^{bw}$. The burst GRB 111228A is not plotted here since its large value defines it as an outlier in the distribution (see text). Neglecting GRB 111228A, the vast majority of SNe (15 SNe) lie in the colored region. Symbols follow Fig. 11.

($v_{ph;peak} = 30\,300 \pm 6000$ km s^{-1}) the corresponding numbers are 1.2 ± 0.3 and 5.7 ± 4.7, respectively. The error is large, in particular for the kinetic energy, which is dominated by the error of $v_{ph;peak}$. As noted above, all values assume $\kappa = \kappa^{bw}$; otherwise these numbers scale accordingly (for a detailed discussion of this issue, see Wheeler et al. 2015).

Finally, we note that neither k_{bol} nor s_{bol} revealed a dependence on redshift. As such there is no redshift dependence of the explosion parameters. These data are fully consistent with the parameter space occupied by the currently known population of GRB SNe, including those at low redshifts, confirming earlier studies (e.g., Soderberg et al. 2006; Tanvir et al. 2010; Sparre et al. 2011).

4.3. Afterglow luminosities

The parameters we have found for the decay slopes α of the afterglows and their spectral slopes β are summarized in Table C.2. These parameters match what has been deduced for other long-duration GRBs (e.g., Zeh et al. 2006; Kann et al. 2006, 2010), α lies between about 0.5 and 1.6, β between about 0.4 and 1.0. Only in the case of GRB 111228A do we see evidence for a potential jet break around 1.7 days after the burst. The observational constraints we can set on the jet-break times for the other three events do not characterize these bursts as special however (for a recent summary of measured jet half-opening angles, see Tanvir et al. 2018). It is possible that in these cases a break is hidden by the rapidly rising SN components and, therefore, remain undetected. Keeping this in mind, the results and constraints we obtain for the beaming-corrected isotropic equivalent energies E_{corr} and jet half-opening angles (Θ_{jet}; Table 3) do not reveal atypical burst parameters. Based on the closure relations between temporal and spectral slopes ($\alpha - \beta$ relations, e.g., Zhang & Mészáros 2004; Gao et al. 2013), in no case can we rule out or favor a wind or an ISM model (Table C.3).

In order to characterize the luminosities of the afterglows, we compare them with the afterglow sample discussed in Kann et al. (2006, 2010, 2011). By using the derived intrinsic slopes of the afterglows as well as the line-of-sight extinctions (which is significantly detected only for GRB 111228A), we applied the method described in Kann et al. (2006) to shift the observed afterglow light curves to a common redshift of $z = 1$.

Table 3. Summary of the afterglow energetics for an ISM and for a wind model.

GRB	Θ_{jet}^{ISM} (deg)	log E_{corr}^{ISM} (erg)	Θ_{jet}^{wind} (deg)	log E_{corr}^{ISM} (erg)
#1	>5.5 ± 0.2	>49.95 ± 0.08	>5.6 ± 0.4	>49.97 ± 0.06
#2	6.3 ± 0.1	50.39 ± 0.04	5.4 ± 0.1	50.26 ± 0.03
#3	>9.5 ± 0.3	>48.90 ± 0.09	>14.5 ± 1.0	>49.26 ± 0.06
#4	>6.8 ± 0.1	>49.70 ± 0.03	>7.6 ± 0.2	>49.80 ± 0.02

Notes. GRB numbers #1 to #4 refer to GRBs 071112C, 111228A, 120714B, and 130831A, respectively. Lower limits on the beaming angle and the corresponding beaming-corrected energy release refer to a break time of t_b >1 day.

We show the afterglow light curves in Fig. 13 (left). These light curves are in Vega magnitudes, in the R_c or the r' band, corrected for Galactic extinction, and, where appropriate, corrected for the contribution of the host galaxy and the late-time SN signature (see Appendix B for details). Other than that, they are as observed. Light-gray afterglows represent the "background sample", which are overwhelmingly those at $z > 1$, though there are some cases where no SN search was undertaken (to our knowledge), or the line-of-sight extinction toward the GRB site prohibited a SN search despite the low redshift (e.g., GRB 130925A, Greiner et al. 2014). The black light curves represent the afterglows of GRBs for which SN signatures have been detected, from late-time red bumps to detailed spectral sequences. We note that several low-z GRB-SN events, such as GRB 980425 (e.g., Galama et al. 1998; Clocchiatti et al. 2011), GRB 031203 (e.g., Malesani et al. 2004), GRB/XRF 060218 (e.g., Pian et al. 2006; Ferrero et al. 2006), and GRB/XRF 100316D (e.g., Cano et al. 2011; Olivares et al. 2012; Bufano et al. 2012) are not included in this sample, as they have no discernable afterglow components (see Kann et al. 2011 for a discussion on upper limits on several of these events)[15]. Finally, we plot the four GRB afterglows discussed in this paper in separate colors and label them.

It can be seen that GRBs which are empirically associated with SNe span a wide variety of behaviors and afterglow magnitudes. At very early times, there are the extremely bright flashes of GRBs 080319B (Racusin et al. 2008; Bloom et al. 2009) and 130427A (Vestrand et al. 2014), but also very faint light curves, like those of XRF 050416A (Kann et al. 2010) and GRB 120714B as presented in this paper. Afterglows of SN-associated GRBs can also be very bright at late times, such as the exceptional case of GRB 030329 (e.g., Lipkin et al. 2004; Kann et al. 2006), and the similarly nearby GRB 130702A (Singer et al. 2013, 2015; Toy et al. 2016; Volnova et al. 2017). This is not unexpected, as there are strong biases involved. All SN-associated GRBs lie at $z \lesssim 1$ and any cases with large line-of-sight extinction (such as GRB 130925A as mentioned above) will not be followed up at late times.

The light curves shifted to $z = 1$ are shown in Fig. 13 (right). Interestingly, the afterglows of GRBs with SN now reside in the lower part of the luminosity distribution, with the exceptions of the aforementioned bright early flashes and a few further cases (e.g., the afterglow of GRB 991208 as well as that of GRB 030329, which is generally not exceptionally luminous,

[15] In the case of GRB/XRF 100316D Olivares et al. (2012) report evidence for an afterglow component in two early-time SEDs.

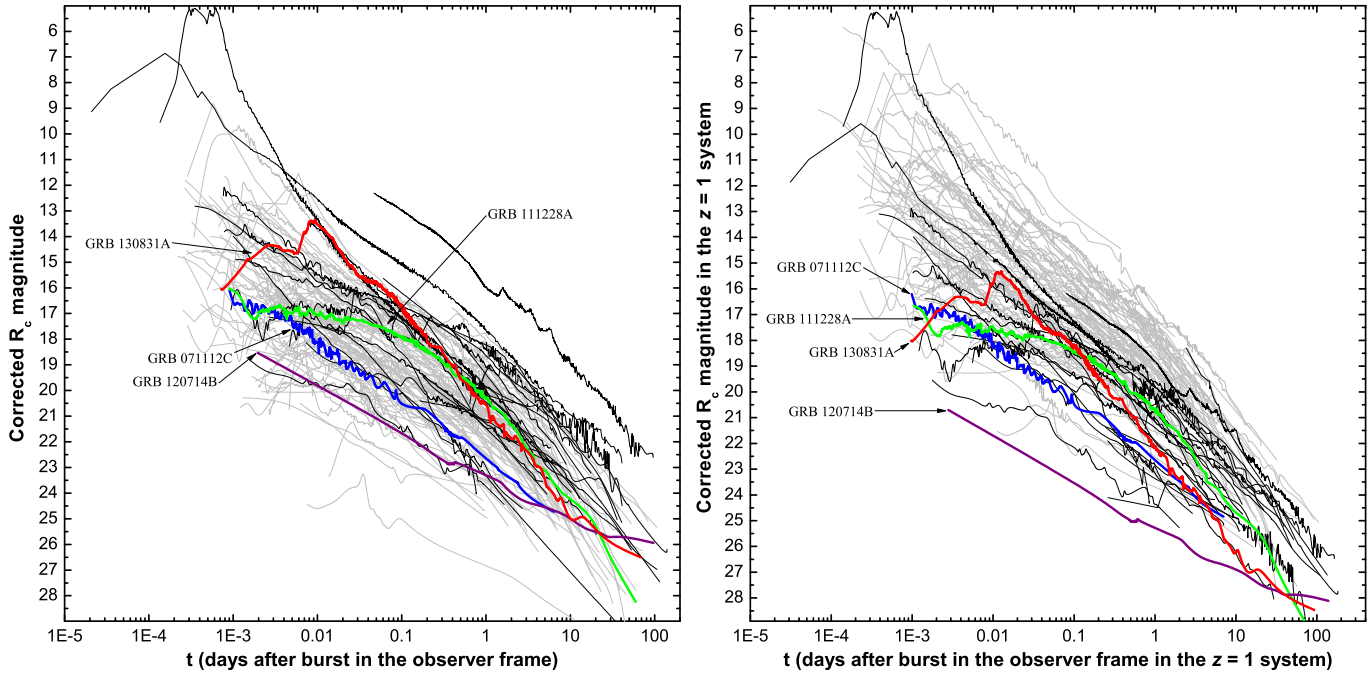

Fig. 13. *Left panel*: observed afterglows of (long) GRBs. These light curves are corrected for Galactic extinction and, where appropriate, for the contribution of the host galaxy and the late-time supernova signature. Light-gray light curves are afterglows with no known SN contribution. Black lines are afterglows with detected SN signatures. Finally, the afterglows of the four GRBs discussed in this paper are color-coded and labeled. It can be seen that GRBs associated with SNe span a large observed magnitude range, from the brightest afterglows to among the faintest. *Right panel*: afterglows, corrected for all line-of-sight extinction, and shifted to a common redshift $z = 1$ (i.e., the afterglows are as they would be observed if they all lay at that redshift and were not affected by dust extinction). The SN-associated GRB afterglows are now seen to cluster in the lower part of the distribution; indeed, GRB 120714B has the least luminous afterglow within the entire sample except at very late times. For more details, see Appendix B.

Kann et al. 2006). Since all long GRBs should be associated with late-time SN emission, this effect of a lower luminosity for GRB SNe might be caused by an observational bias. In particular, only a low redshift enables detailed observations of even intrinsically low-luminosity afterglows. One such case is GRB 120714B, which is found to be the least luminous afterglow in the entire sample for most of its observed time span; at $t \sim 0.03$ days (in the $z = 1$ system) it was more than 12 mag less luminous than the brightest afterglows at that time and at $t = 1$ day it was still ∼5 mag fainter than the median of the distribution; a clear advantage for the monitoring of the SN bump.

4.4. Host-galaxy properties

The host-galaxy magnitudes in our sample range between $r' = 23$ and 25 mag (AB system), the brightest being the one of GRB 120714B, which is also the closest. On the GROND images all hosts appear mostly featureless; their morphology is not revealed. Additional archival *Hubble* Space Telescope (HST) data in the case of GRB 071112C as well as observations with the High Acuity Wide field K-band Imager (HAWKI) mounted at the VLT (GRB 120714B) and deep imaging with FORS2 (GRB 130831A) do not show any substructure either. An astrometry of these images shows that three of the four GRB SNe exploded within the inner 1−2 kpc projected distance from the geometric center of their hosts.

In order to measure the (global) SFR in the hosts, we modeled their Galactic-extinction-corrected broad-band SEDs (Table C.4) using `Le PHARE` (Arnouts et al. 1999; Ilbert et al. 2006)[16] (PHotometric Analysis for Redshift Estimations) by applying a grid of galaxy templates based on Bruzual & Charlot (2003) stellar population-synthesis models with the Chabrier initial mass function.

All four host galaxies (Fig. 14) turn out to be rather typical members of the class of long-GRB hosts as they are found in the low-z universe ($z = 0.4 - 0.8$; look-back time between ∼4.4 and 7.1 Gyr; Table C.5). They are low-luminosity ($M_B = -18.6$ to -17.7), low-mass ($\log M/M_\odot = 8.4 - 8.7$) hosts. Their global SFR is relatively modest, on the order of 1 $M_\odot\,\mathrm{yr}^{-1}$. Their specific SFR (sSFR) is (within the errors) relatively normal when compared to the $z < 0.5$ GRB host-galaxy sample studied by Vergani et al. (2015) and Schulze et al. (2018), log sSFR ∼−8.7 to −8.4 ($M_\odot\,\mathrm{yr}^{-1}$ per $M_\odot$), suggesting that all four galaxies are undergoing episodes of star-forming activity. Their global parameters (M_B, SFR, $M/M_\odot$) lie close to the median found for the *Swift*/BAT6 GRB host-galaxy sample of long GRBs (Vergani et al. 2015).

Nevertheless, some caution is required concerning the deduced SFR: Due to the lack of HK_s detections for the hosts of GRBs 111228A and 130831A, in these cases the stellar mass and sSFR obtained by `Le PHARE` should be taken with care.

5. Summary

We have performed a detailed study of the GRB SNe related to the long GRBs 071112C, 111228A, 120714B, and 130831A, covering a redshift range from $z = 0.4$ to 0.8. Partly in combination with public data, we were able to follow their light curves in $g'r'i'z'$ over several weeks, with additional host-galaxy observations more than one year after the corresponding burst. These events belong to a rare number of fewer than 20 GRB SNe for

[16] http://www.cfht.hawaii.edu/~arnouts/LEPHARE

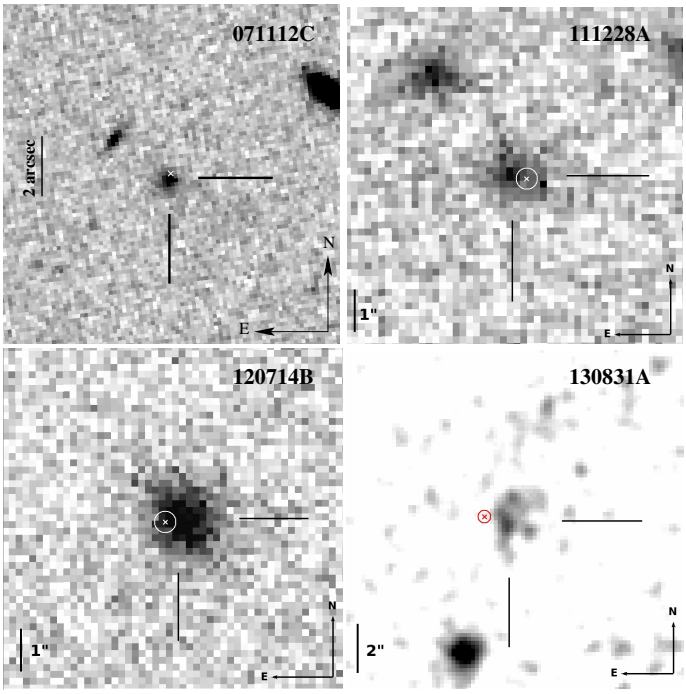

Fig. 14. The four GRB host galaxies: *top left panel*: archived HST/WFC3 F160W image taken 3 years after the burst (HST proposal ID 12307, PI: A. J. Levan); *top right panel*: GROND $g'r'i'z'$ combined white-band; *bottom left panel*: GROND $g'r'i'z'$ combined white-band; and *bottom right panel*: GROND $g'r'$ combined.

which multi-color light curves in at least three photometric bands are available. This allowed us to derive (quasi-) bolometric light-curve parameters (stretch factor $s_{\rm bol}$ and luminosity factor $k_{\rm bol}$) and, using the Arnett SN model, to determine the SN explosion parameters $M_{\rm Ni}$ and $M_{\rm ej}^3/E_{\rm kin}$ normalized to the corresponding parameters of SN 1998bw. In doing so, we found that the four SNe studied here released between 0.5 and 1.0 $M_\odot$ of radioactive nickel, a parameter range which lies within the observed interval for GRB SNe at low and medium redshifts ($z = 0.1 - 0.9$). For $M_{\rm ej}^3/E_{\rm kin}$ the parameter range is larger, between 0.5 and 6.3. However, this large range is mainly affected by the outlier GRB 111228A, whose high value (6.3) could be a consequence of the relatively flat SN bump that made the precise determination of its bolometric stretch factor difficult. Omitting this burst, for the other three events we have found $0.5 \lesssim M_{\rm ej}^3/E_{\rm kin} \lesssim 0.8$, a range which is consistent with the parameter space occupied by the presently known GRB–SN ensemble with multi-color light-curve data.

Among our sample, GRB 120714B/SN 2012eb at $z = 0.40$ turned out to be of particular interest. It belongs to the subclass of intermediate-luminosity GRBs, has the least luminous optical afterglow among all well-observed long-duration GRBs, and showed evidence for a black-body component in its optical transient at early times. In addition, VLT/FORS2 spectroscopy revealed a photospheric expansion velocity of $v_{\rm ph} \sim 40\,000\,{\rm km\,s^{-1}}$ close to SN maximum (based on the Si II feature). This is the highest expansion velocity found so far for a GRB SN close to maximum light. In contrast to this high value, for GRB 130831A/SN 2013fu using the Fe II λ4570 feature we measure $v_{\rm ph} \sim 20\,000\,{\rm km\,s^{-1}}$ near peak time, a value close to the lower end of the observed distribution of $v_{\rm ph}$ for GRB SNe measured via the iron features.

The fact that GRB 120714B/SN 2012eb was an intermediate-luminosity burst that showed a black-body component in its optical transient fits into the picture (Bromberg et al. 2011) that there is a continuum between low- and high-luminosity GRBs (Schulze et al. 2014; for a review see also Cano et al. 2017 and references therein). The case of SN 2012eb also makes clear that a systematic search for such a black-body component in GRB-SN light curves in the optical bands (observer frame) might be a challenging task. On the one hand it requires early-time data which reach into the UV band in the GRB host frame, that is, the higher the cosmological redshift the better. On the other hand, it requires a bright thermal component and a correspondingly faint afterglow and underlying host galaxy.

We have shown that GRB SNe at moderately high redshifts can be well-studied with 2 m-class optical telescopes, provided good observing sites and instrumentation. Based on ten years of GROND multi-color follow-up observing campaigns at the MPG 2.2m telescope on ESO/La Silla, altogether nine GRB SNe have now been investigated in detail in the optical $g'r'i'z'$ bands. Most of these were discovered with GROND. Even though on average this is just one event per year, in total it represents 20% of the currently known GRB SN sample.

Acknowledgements. S.K., Sebastian S., and A.N.G. acknowledge support by the Thüringer Ministerium für Bildung, Wissenschaft und Kultur under FKZ 12010-514. S.K., Sebastian S., A.N.G., and D.A.K. acknowledge support by grant DFG Kl 766/16-3. A.N.G., A.R., D.A.K., and A.U. are grateful for travel funding support through MPE Garching. A.R. acknowledges additional support by the Jenaer Graduiertenakademie, by TLS Tautenburg and DFG Kl/766 13-2. D.A.K. acknowledges support by TLS Tautenburg and MPE Garching, as well as support from the Spanish research project AYA 2014-58381-P and Juan de la Cierva Incorporación IJCI-2015-26153. P.S. and T.K. acknowledges support through the Sofja Kovalevskaja Award to P.S. from the Alexander von Humboldt Foundation of Germany. R.F. acknowledges support from European Regional Development Fund-Project "Engineering applications of microworld physics" (No. CZ.02.1.01/0.0/0.0/16_019/0000766). F.O.E. acknowledge support from the FONDECYT grant #11170953. Support for F.O.E. is provided by the Ministry of Economy, Development, and Tourism's Millennium Science Initiative through grant IC120009, awarded to The Millennium Institute of Astrophysics, MAS. The Cosmic Dawn center is funded by the DNRF. Part of the funding for GROND (both hardware and personnel) was generously granted by the Leibniz-Prize to G. Hasinger (DFG grant HA 1850/28-1). This work made use of data supplied by the UK *Swift* science data center at the University of Leicester. This work is based in part on observations made with the *Spitzer* Space Telescope, which is operated by the Jet Propulsion Laboratory, California Institute of Technology under a contract with NASA. Support for this work was provided by NASA through an award issued by JPL/Caltech. Some of the data presented herein were obtained at the W. M. Keck Observatory, which is operated as a scientific partnership among the California Institute of Technology, the University of California and the National Aeronautics and Space Administration. The Observatory was made possible by the generous financial support of the W. M. Keck Foundation. The authors wish to recognize and acknowledge the very significant cultural role and reverence that the summit of Maunakea has always had within the indigenous Hawaiian community. We thank Dan Perley for generously providing these Keck telescope data as well as *Spitzer* Space Telescope data. We thank the referee for a very constructive report.

References

Abazajian, K. N., Adelman-McCarthy, J. K., Agüeros, M. A., et al. 2009, ApJS, 182, 543
Alam, S., Albareti, F. D., Allende Prieto, C., et al. 2015, ApJS, 219, 12
Arnett, W. D. 1982, ApJ, 253, 785
Arnouts, S., Cristiani, S., Moscardini, L., et al. 1999, MNRAS, 310, 540
Barthelmy, S. D., Barbier, L. M., Cummings, J. R., et al. 2005, Space Sci. Rev., 120, 143
Barthelmy, S. D., Baumgartner, W. H., Cummings, J. R., et al. 2013, GRB Coordinates Netw., 15155, 1
Ben-Ami, S., Gal-Yam, A., Filippenko, A. V., et al. 2012, ApJ, 760, L33
Bloom, J. S., Frail, D. A., & Kulkarni, S. R. 2003, ApJ, 594, 674

Bloom, J. S., Perley, D. A., Li, W., et al. 2009, ApJ, 691, 723
Briggs, M. S., & Younes, G. 2011, GRB Coordinates Netw., 12744, 1
Bromberg, O., Nakar, E., & Piran, T. 2011, ApJ, 739, L55
Bruzual, G., & Charlot, S. 2003, MNRAS, 344, 1000
Bufano, F., Pian, E., Sollerman, J., et al. 2012, ApJ, 753, 67
Burenin, R., Khamitov, I., Pavlinsky, M., et al. 2007, GRB Coordinates Netw., 7066, 1
Butler, N. R., Kocevski, D., Bloom, J. S., & Curtis, J. L. 2007, ApJ, 671, 656
Campana, S., Mangano, V., Blustin, A. J., et al. 2006, Nature, 442, 1008
Cano, Z. 2013, MNRAS, 434, 1098
Cano, Z. 2014, ApJ, 794, 121
Cano, Z., Bersier, D., Guidorzi, C., et al. 2011, ApJ, 740, 41
Cano, Z., de Ugarte Postigo, A., Pozanenko, A., et al. 2014, A&A, 568, A19
Cano, Z., Wang, S.-Q., Dai, Z.-G., & Wu, X.-F. 2017, Adv. Astron., 2017, 8929054
Chevalier, R. A., & Li, Z.-Y. 2000, ApJ, 536, 195
Clocchiatti, A., Suntzeff, N. B., Covarrubias, R., & Candia, P. 2011, AJ, 141, 163
Cobb, B. E. 2012, in Death of Massive Stars: Supernovae and Gamma-Ray Bursts, IAU Symp., 279, 83
Cobb, B. E., Bailyn, C. D., van Dokkum, P. G., Buxton, M. M., & Bloom, J. S. 2004, ApJ, 608, L93
Cobb, B. E., Bailyn, C. D., van Dokkum, P. G., & Natarajan, P. 2006, ApJ, 645, L113
Covino, S., Melandri, A., Salvaterra, R., et al. 2013, MNRAS, 432, 1231
Cucchiara, A., & Levan, A. J. 2011, GRB Coordinates Netw., 12761, 1
Cucchiara, A., & Perley, D. 2013, GRB Coordinates Netw., 15144, 1
Cummings, J. R., Barthelmy, S. D., Baumgartner, W. H., et al. 2011, GRB Coordinates Netw., 12749, 1
Cummings, J. R., Barthelmy, S. D., Baumgartner, W. H., et al. 2012, GRB Coordinates Netw., 13481, 1
D'Avanzo, P., Melandri, A., Palazzi, E., et al. 2012, GRB Coordinates Netw., 13069, 1
D'Elia, V., Pian, E., Melandri, A., et al. 2015, A&A, 577, A116
Della Valle, M., Malesani, D., Benetti, S., Testa, V., & Stella, L. 2003a, IAU Circ., 8197, 2
Della Valle, M., Malesani, D., Benetti, S., et al. 2003b, A&A, 406, L33
Della Valle, M., Chincarini, G., Panagia, N., et al. 2006, Nature, 444, 1050
De Pasquale, M., Oates, S. R., Racusin, J. L., et al. 2016, MNRAS, 455, 1027
Dessart, L., Hillier, D. J., Woosley, S., et al. 2016, MNRAS, 458, 1618
Dessart, L., John Hillier, D., Yoon, S.-C., Waldman, R., & Livne, E. 2017, A&A, 603, A51
de Ugarte Postigo, A., Thöne, C. C., Bensch, K., et al. 2018, A&A, 620, A190
Dintinjana, B., Maticic, S., Mikuz, H., & Skvarc, J. 2007, GRB Coordinates Netw., 7078, 1
Dittmann, J., Laskar, T., & Berger, E. 2011, GRB Coordinates Netw., 12759, 1
Evans, P. A., Beardmore, A. P., Page, K. L., et al. 2007, A&A, 469, 379
Ferrero, P., Kann, D. A., Zeh, A., et al. 2006, A&A, 457, 857
Fisher, A., Branch, D., Nugent, P., & Baron, E. 1997, ApJ, 481, L89
Förster, F., Maureira, J. C., San Martín, J., et al. 2016, ApJ, 832, 155
Frail, D. A., Kulkarni, S. R., Sari, R., et al. 2001, ApJ, 562, L55
Fynbo, J. P. U., Watson, D., Thöne, C. C., et al. 2006, Nature, 444, 1047
Fynbo, J. P. U., Jakobsson, P., Prochaska, J. X., et al. 2009, ApJS, 185, 526
Fynbo, J. P. U., Malesani, D., & Jakobsson, P. 2012a, in Long Gamma-Ray Burst Host Galaxies and their Environments, eds. C. Kouveliotou, R. A. M. J. Wijers, & S. Woosley, 269
Fynbo, J. P. U., de Ugarte Postigo, A., D'Elia, V., Xu, D., & Malesani, D. 2012b, GRB Coordinates Netw., 13477, 1
Galama, T. J., Vreeswijk, P. M., van Paradijs, J., et al. 1998, Nature, 395, 670
Gal-Yam, A., Moon, D.-S., Fox, D. B., et al. 2004, ApJ, 609, L59
Gal-Yam, A., Fox, D. B., Price, P. A., et al. 2006, Nature, 444, 1053
Gao, H., Lei, W.-H., Zou, Y.-C., Wu, X.-F., & Zhang, B. 2013, New Astron. Rev., 57, 141
Gehrels, N., Chincarini, G., Giommi, P., et al. 2004, ApJ, 611, 1005
Golenetskii, S., Aptekar, R., Frederiks, D., et al. 2011, GRB Coordinates Netw., 12790, 1
Golenetskii, S., Aptekar, R., Frederiks, D., et al. 2013, GRB Coordinates Netw., 15145, 1
Gorbovskoy, E., Lipunov, V., Tyurina, N., et al. 2015, GRB Coordinates Netw., 18673, 1
Greco, G., Terra, F., Bartolini, C., et al. 2007, GRB Coordinates Netw., 7089, 1
Greiner, J., Bornemann, W., Clemens, C., et al. 2007, The Messenger, 130, 12
Greiner, J., Bornemann, W., Clemens, C., et al. 2008, PASP, 120, 405
Greiner, J., Yu, H.-F., Krühler, T., et al. 2014, A&A, 568, A75
Greiner, J., Mazzali, P. A., Kann, D. A., et al. 2015, Nature, 523, 189
Guillochon, J., Parrent, J., Kelley, L. Z., & Margutti, R. 2017, ApJ, 835, 64
Hagen, L. M. Z., Chester, M. M., Cummings, J. R., et al. 2013, GRB Coordinates Netw., 15139, 1
Hjorth, J. 2013, Phil. Trans. R. Soc. London Ser. A, 371, 20120275
Hjorth, J., & Bloom, J. S. 2012, The Gamma-Ray Burst – Supernova Connection (Cambridge: Cambridge University Press), 169
Huang, K. Y., Urata, Y., Tung, Y. H., et al. 2012, ApJ, 748, 44
Ilbert, O., Arnouts, S., McCracken, H. J., et al. 2006, A&A, 457, 841
Irwin, C. M., & Chevalier, R. A. 2016, MNRAS, 460, 1680
Ishimura, T., Shimokawabe, T., Mori, Y., et al. 2007, GRB Coordinates Netw., 7087, 1
Izzo, L., Thöne, C. C., Schulze, S., et al. 2017, MNRAS, 472, 4480
Jakobsson, P., Fynbo, J. P. U., Malesani, D., et al. 2007, GRB Coordinates Netw., 7088, 1
Kann, D. A., Klose, S., & Zeh, A. 2006, ApJ, 641, 993
Kann, D. A., Klose, S., Zhang, B., et al. 2010, ApJ, 720, 1513
Kann, D. A., Klose, S., Zhang, B., et al. 2011, ApJ, 734, 96
Kann, D. A., Schady, P., Olivares, E. F., et al. 2016, A&A, submitted [arXiv:1606.06791]
Kann, D. A., Schady, P., Olivares, E. F., et al. 2018, A&A, 617, A122
Khorunzhev, G., Burenin, R., Pavlinsky, M., et al. 2013, GRB Coordinates Netw., 15244, 1
Klose, S. 2017, ApJ, submitted
Klose, S., Greiner, J., & Fynbo, J. 2012a, GRB Coordinates Netw., 13613, 1
Klose, S., Greiner, J., Fynbo, J., et al. 2012b, Cent. Bureau Electron. Telegr., 3200, 1
Klose, S., Nicuesa Guelbenzu, A., & Kruehler, T. 2013a, GRB Coordinates Netw., 15320, 1
Klose, S., Nicuesa Guelbenzu, A., Kruehler, T., et al. 2013b, Cent. Bureau Electron. Telegr., 3677, 1
Klotz, A., Boer, M., & Atteia, J. L. 2007, GRB Coordinates Netw., 7065, 1
Kocevski, D., Modjaz, M., Bloom, J. S., et al. 2007, ApJ, 663, 1180
Krimm, H., Barbier, L., Barthelmy, S., et al. 2007, GRB Coordinates Netw., 7081, 1
Krühler, T., Küpcü Yoldaş, A., Greiner, J., et al. 2008, ApJ, 685, 376
Krühler, T., Malesani, D., Fynbo, J. P. U., et al. 2015, A&A, 581, A125
Krühler, T., Kuncarayakti, H., Schady, P., et al. 2017, A&A, 602, A85
Lipkin, Y. M., Ofek, E. O., Gal-Yam, A., et al. 2004, ApJ, 606, 381
Lü, H. J., Lan, L., Zhang, B., et al. 2018, ApJ, 862, 130
Lupton, R. H., Jurić, M., Ivezić, Z., et al. 2005, BAAS, 37, 1384
Malesani, D., Tagliaferri, G., Chincarini, G., et al. 2004, ApJ, 609, L5
Marshall, F. E., & Saxton, C. J. 2012, GRB Coordinates Netw., 13473, 1
Masetti, N., Palazzi, E., Pian, E., et al. 2005, A&A, 438, 841
Mazzali, P. A., Deng, J., Pian, E., et al. 2006, ApJ, 645, 1323
Mazzali, P. A., Walker, E. S., Pian, E., et al. 2013, MNRAS, 432, 2463
Mazzali, P. A., McFadyen, A. I., Woosley, S. E., Pian, E., & Tanaka, M. 2014, MNRAS, 443, 67
Mazzali, P. A., Sullivan, M., Pian, E., Greiner, J., & Kann, D. A. 2016, MNRAS, 458, 3455
Meegan, C., Lichti, G., Bhat, P. N., et al. 2009, ApJ, 702, 791
Melandri, A., Pian, E., D'Elia, V., et al. 2014, A&A, 567, A29
Mesler, R. A., Whalen, D. J., Smidt, J., et al. 2014, ApJ, 787, 91
Michałowski, M. J., Kamble, A., Hjorth, J., et al. 2012, ApJ, 755, 85
Michałowski, M. J., Xu, D., Stevens, J., et al. 2018, A&A, 616, A169
Minezaki, T., Price, P. A., Yoshii, Y., & Cowie, L. L. 2007, GRB Coordinates Netw., 7135, 1
Nakamura, T., Mazzali, P. A., Nomoto, K., & Iwamoto, K. 2001, ApJ, 550, 991
Nakar, E., & Sari, R. 2010, ApJ, 725, 904
Nicuesa Guelbenzu, A., Klose, S., & Greiner, J. 2011, GRB Coordinates Netw., 12757, 1
Nicuesa Guelbenzu, A. M., Klose, S., & Greiner, J. 2012, GRB Coordinates Netw., 13478, 1
Niino, Y., Hashimoto, T., Aoki, K., et al. 2012, PASJ, 64, 115
Oates, S. R., & Stratta, G. 2007, GRB Coordinates Netw., 7080, 1
Olivares, E. F., Greiner, J., Schady, P., et al. 2012, A&A, 539, A76
Olivares, E. F., Greiner, J., Schady, P., et al. 2015, A&A, 577, A44
Palazzi, E., Fugazza, D., & Piranomonte, S. 2011, GRB Coordinates Netw., 12765, 1
Patat, F., Cappellaro, E., Danziger, J., et al. 2001, ApJ, 555, 900
Pei, Y. C. 1992, ApJ, 395, 130
Perley, D. A., Krühler, T., Schulze, S., et al. 2016a, ApJ, 817, 7
Perley, D. A., Tanvir, N. R., Hjorth, J., et al. 2016b, ApJ, 817, 8
Perley, D., Berger, E., Butler, N., et al. 2016c, The Spitzer/Swift Gamma-Ray Burst Host Galaxy Legacy Survey, Spitzer Proposal
Perri, M., Stratta, G., Barthelmy, S. D., et al. 2007, GRB Coordinates Netw., 7059, 1
Pian, E., Mazzali, P. A., Masetti, N., et al. 2006, Nature, 442, 1011
Poole, T. S., Breeveld, A. A., Page, M. J., et al. 2008, MNRAS, 383, 627
Prentice, S. J., Mazzali, P. A., Pian, E., et al. 2016, MNRAS, 458, 2973
Racusin, J. L., Karpov, S. V., Sokolowski, M., et al. 2008, Nature, 455, 183
Rhoads, J. E. 1999, ApJ, 525, 737

Roming, P. W. A., Kennedy, T. E., Mason, K. O., et al. 2005, Space Sci. Rev., 120, 95
Rossi, A., Schulze, S., Klose, S., et al. 2011, A&A, 529, A142
Rossi, A., Klose, S., Ferrero, P., et al. 2012, A&A, 545, A77
Ruffini, R., Vereshchagin, G. V., & Wang, Y. 2017, A&A, 600, A131
Sanders, N. E., Soderberg, A. M., Valenti, S., et al. 2012, ApJ, 756, 184
Sari, R., Piran, T., & Halpern, J. P. 1999, ApJ, 519, L17
Saxton, C. J., Barthelmy, S. D., Baumgartner, W. H., et al. 2012, GRB Coordinates Netw., 13471, 1
Schady, P., de Pasquale, M., Page, M. J., et al. 2007, MNRAS, 380, 1041
Schlafly, E. F., & Finkbeiner, D. P. 2011, ApJ, 737, 103
Schulze, S., Covino, S., Flores, H., et al. 2011, GRB Coordinates Netw., 12770, 1
Schulze, S., Malesani, D., Cucchiara, A., et al. 2014, A&A, 566, A102
Schulze, S., Krühler, T., Leloudas, G., et al. 2018, MNRAS, 473, 1258
Singer, L. P., Cenko, S. B., Kasliwal, M. M., et al. 2013, ApJ, 776, L34
Singer, L. P., Kasliwal, M. M., Cenko, S. B., et al. 2015, ApJ, 806, 52
Skrutskie, M. F., Cutri, R. M., Stiening, R., et al. 2006, AJ, 131, 1163
Soderberg, A. M., Kulkarni, S. R., Price, P. A., et al. 2006, ApJ, 636, 391
Sparre, M., & Starling, R. L. C. 2012, MNRAS, 427, 2965
Sparre, M., Sollerman, J., Fynbo, J. P. U., et al. 2011, ApJ, 735, L24
Spergel, D. N., Verde, L., Peiris, H. V., et al. 2003, ApJS, 148, 175
Sposetti, S. 2007, GRB Coordinates Netw., 7090, 1
Stanek, K. Z., Garnavich, P. M., Nutzman, P. A., et al. 2005, ApJ, 626, L5
Starling, R. L. C., Wiersema, K., Levan, A. J., et al. 2011, MNRAS, 411, 2792
Starling, R. L. C., Page, K. L., Pe'Er, A., Beardmore, A. P., & Osborne, J. P. 2012, MNRAS, 427, 2950
Stritzinger, M., & Leibundgut, B. 2005, A&A, 431, 423
Takaki, K., Kawabata, K. S., Yamanaka, M., et al. 2013, ApJ, 772, L17
Tanga, M., Krühler, T., Schady, P., et al. 2018, A&A, 615, A136
Tanvir, N. R., Rol, E., Levan, A. J., et al. 2010, ApJ, 725, 625
Tanvir, N. R., Laskar, T., Levan, A. J., et al. 2018, ApJ, 865, 107
Thöne, C. C., de Ugarte Postigo, A., Fryer, C. L., et al. 2011, Nature, 480, 72
Thöne, C. C., Christensen, L., Prochaska, J. X., et al. 2014, MNRAS, 441, 2034
Tinney, C., Stathakis, R., Cannon, R., et al. 1998, IAU Circ., 6896, 1
Tody, D. 1986, in Instrumentation in Astronomy VI, ed. D. L. Crawford, SPIE Conf. Ser., 627, 733
Tody, D. 1993, ASP Conf. Ser., 52, 173
Tomita, H., Deng, J., Maeda, K., et al. 2006, ApJ, 644, 400
Toy, V. L., Cenko, S. B., Silverman, J. M., et al. 2016, ApJ, 818, 79
Uehara, T., Uemura, M., Kawabata, K. S., et al. 2010, A&A, 519, A56
Ukwatta, T. N., Baumgartner, W. H., Burrows, D. N., et al. 2011, GRB Coordinates Netw., 12737, 1
Valenti, S., Benetti, S., Cappellaro, E., et al. 2008, MNRAS, 383, 1485
Vergani, S. D., Salvaterra, R., Japelj, J., et al. 2015, A&A, 581, A102
Vestrand, W. T., Wren, J. A., Panaitescu, A., et al. 2014, Science, 343, 38
Volnova, A. A., Pruzhinskaya, M. V., Pozanenko, A. S., et al. 2017, MNRAS, 467, 3500
Wang, L. J., Yu, H., Liu, L. D., et al. 2017, ApJ, 837, 128
Waxman, E., Mészáros, P., & Campana, S. 2007, ApJ, 667, 351
Wheeler, J. C., Johnson, V., & Clocchiatti, A. 2015, MNRAS, 450, 1295
Xin, L.-P., Wang, Y.-Z., Lin, T.-T., et al. 2016, ApJ, 817, 152
Xu, D., Starling, R. L. C., Fynbo, J. P. U., et al. 2009, ApJ, 696, 971
Xu, D., Fynbo, J. P. U., McCormac, J., & Jakobsson, P. 2011, GRB Coordinates Netw., 12764, 1
Xu, D., de Ugarte Postigo, A., Leloudas, G., et al. 2013, ApJ, 776, 98
Yaron, O., & Gal-Yam, A. 2012, PASP, 124, 668
Yoldaş, A. K., Krühler, T., & Greiner, J. 2008, in AIP Conf. Ser., eds. M. Galassi, D. Palmer, & E. Fenimore, 1000, 227
Yoshida, M., Yanagisawa, K., Shimizu, Y., et al. 2007, GRB Coordinates Netw., 7091, 1
Yuan, F., Rykoff, E. S., Rujopakarn, W., & Swan, H. 2007, GRB Coordinates Netw., 7061, 1
Zeh, A., Klose, S., & Hartmann, D. H. 2004, ApJ, 609, 952
Zeh, A., Kann, D. A., Klose, S., & Hartmann, D. H. 2005a, Nuovo Cimento C Geophys. Space Phys. C, 28, 617
Zeh, A., Klose, S., & Hartmann, D. H. 2005b, in 22nd Texas Symposium on Relativistic Astrophysics, eds. P. Chen, E. Bloom, G. Madejski, & V. Patrosian, 574
Zeh, A., Klose, S., & Kann, D. A. 2006, ApJ, 637, 889
Zhang, B., & Mészáros, P. 2004, Int. J. Mod. Phys. A, 19, 2385
Zhang, Q., Huang, Y. F., & Zong, H. S. 2016, ApJ, 823, 156

[1] Thüringer Landessternwarte Tautenburg, Sternwarte 5, 07778 Tautenburg, Germany
e-mail: klose@tls-tautenburg.de
[2] Instituto de Astrofísica de Andalucía (IAA-CSIC), Glorieta de la Astronomía s/n, 18008 Granada, Spain
[3] Department of Particle Physics and Astrophysics, Weizmann Institute of Science, Rehovot 76100, Israel
[4] Instituto de Astrofísica, Facultad de Física, Pontificia Universidad Católica de Chile, 306, Santiago 22, Chile
[5] Millennium Institute of Astrophysics (MAS), Nuncio Monseñor Sótero Sanz 100, Providencia, Santiago, Chile
[6] Max-Planck-Institut für Extraterrestrische Physik, Giessenbachstraße 1, 85748 Garching, Germany
[7] Departamento de Astronomía, Universidad de Chile, Camino el Observatorio 1515, Santiago, Chile
[8] American River College, Department of Physics and Astronomy, 4700 College Oak Drive, Sacramento CA, 95841, USA
[9] Institute of Experimental and Applied Physics, Czech Technical University in Prague, Horska 3a/22, 128 00 Prague 2, Czech Republic
[10] Astrophysics Research Institute, Liverpool John Moores University, IC2, Liverpool Science Park, 146 Brownlow Hill, Liverpool L3 5RF, UK
[11] INAF-OAS Bologna, Via Gobetti 93/3, 40129 Bologna, Italy
[12] Department of Chemistry and Physics, Roger Williams University, One Old Ferry Road, Bristol, RI 02809, USA

Appendix A: Details on the individual bursts

A.1. GRB 071112C

The burst and the afterglow data. The burst was detected by the *Swift* Burst Alert Telescope (BAT; Barthelmy et al. 2005) on 2007 Nov 12 at 18:32:57 UT (Perri et al. 2007). It consisted of a single peak (FRED-like: fast-rise, exponential decay) with a duration of $T_{90}(15-350\,\mathrm{keV}) = 15\pm2$ s (Krimm et al. 2007). The optical afterglow was discovered by *Swift*/UVOT (Perri et al. 2007). Based on a spectrum of the afterglow with FORS2 a redshift of $z = 0.823$ was found (Jakobsson et al. 2007). The properties of the burst and its early afterglow based on data available at the time are summarized in detail in Kann et al. (2010).

The multi-channel imager GROND was on target starting about 8 h after the burst and continued visiting the field for another seven epochs, spanning a time span of 28 days in total. The late-time GROND data (Table C.6) reveal a pronounced SN bump in the $r'i'z'$ bands with its peak being about 2 weeks after the burst (Fig. 1). This is the most distant GRB SN in our sample.

At the time when the GRB went off, the field of the burst was immediately observable from Europe to East Asia, resulting in a well-covered early light curve of the optical transient. Early observations ($t > 90$ s) are discussed in Uehara et al. (2010) and Huang et al. (2012). For the construction of the light curve of the optical transient we took data from those two papers, as well as Covino et al. (2013), Fynbo et al. (2009), the UVOT automatic analysis page[17], the GCN Circulars (Yuan et al. 2007; Klotz et al. 2007; Burenin et al. 2007; Dintinjana et al. 2007; Oates & Stratta 2007; Ishimura et al. 2007; Greco et al. 2007; Sposetti 2007; Yoshida et al. 2007, and Minezaki et al. 2007). With the exception of a single measurement from Covino et al. (2013), we are unaware of any other observations between one day post-burst and late-time host-galaxy data. Late host-galaxy data are taken from Vergani et al. (2015). We note that there is a difference of an entire magnitude between late-time host-galaxy magnitudes as given in Huang et al. (2012) and Vergani et al. (2015). Our GROND observations yield an intermediate value. We do not use the value from Huang et al. (2012). We also do not use late-time i'-band data from Covino et al. (2013), which is significantly brighter than our own data during the SN epoch as well as the re-reduction in Vergani et al. (2015).

Afterglow properties. In our analysis we included data from the literature beginning 0.06 days after the GRB. The fit in $g'r'i'z'$ then gives $\alpha = 0.96 \pm 0.01$. When compared with the results of the statistical study of afterglow light curves by Zeh et al. (2006) this suggests that for the considered time span the fireball was in the pre-break evolutionary phase. An identical fit result was reported by Huang et al. (2012), who used optical data until about $t = 1$ day to fit their light curve.

Assuming for the jet break time $t_b > 1$ day and using the observed isotropic equivalent energy (Table 1), this constrains the jet half-opening angle to $\Theta_{\rm ISM} > 5.5\pm0.2$ deg for an ISM and $\Theta_{\rm wind} > 5.6 \pm 0.4$ deg for a wind model, and implies a beaming-corrected energy release (in units of erg) of $\log E_{\rm corr,ISM}[\mathrm{erg}] > 49.95 \pm 0.08$ and $\log E_{\rm corr,wind}[\mathrm{erg}] > 49.97 \pm 0.06$, respectively.

Based on GROND $g'r'i'z'JHK_s$ data the SED of the afterglow does not show evidence for host-galaxy extinction (Table C.2, Fig. A.1). The observed decay slope ($\alpha = 0.96\pm0.01$) and the obvious lack of a break in the light curve until at least 2–3 days after the burst suggest that our α,β measurements refer to the spherical expansion phase. The α–β relations

[17] http://swift.gsfc.nasa.gov/uvot_tdrss/296504/index.html

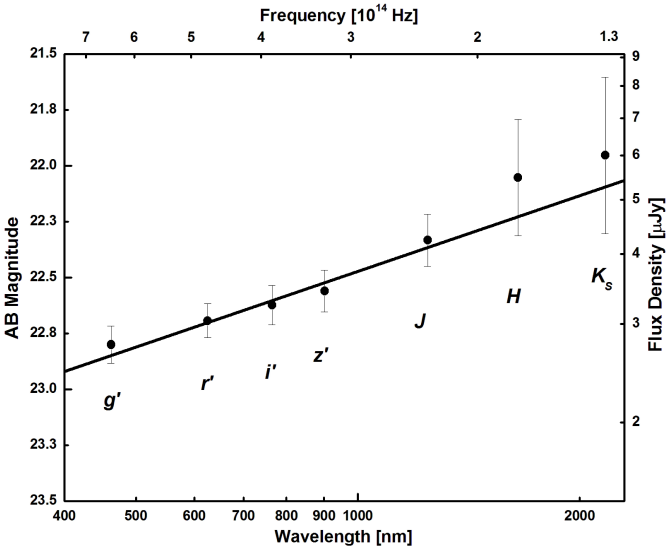

Fig. A.1. SED of the afterglow of GRB 071112C based on GROND multi-color data and a joint fit of the $g'r'i'z'$-band light curves, assuming a simple power-law decay. Magnitudes refer to $t = 1$ day (corrected for Galactic extinction). The SED is well-described by a pure power-law, i.e., it does not show evidence for host-galaxy extinction.

(Zhang & Mészáros 2004) then show that during this phase the cooling frequency was above the optical bands, $\nu_{\rm obs} < \nu_c$, in agreement with the results reported by Huang et al. (2012). A wind model is preferred over an ISM model, although the latter model is not ruled out (Table C.3).

Host galaxy properties. The GRB host galaxy was observed with GROND seven years after the burst. It turned out to be rather faint (Table C.2). In order to measure the position of the optical transient with respect to its host galaxy, we made use of archival HST/Wide Field Camera 3 (WFC3) F160W images taken 3 years after the burst (HST proposal ID 12307, PI: A. J. Levan, see Vergani et al. 2015). We astrometrized these images using the `Gaia` package and compared them with the GROND images. We find that the optical transient was placed $0\farcs26\pm0\farcs20$ (2.1 ± 1.6 kpc) away from the brightness center of its host, which on the HST image (centered at a wavelength of 8800 Å in the rest frame) does not reveal any substructure (Fig. 14). We note that on the HST image a lenticular galaxy of roughly similar brightness and angular extension lies only $2\farcs0$ north-east of the GRB host, though no redshift information is available for this galaxy meaning that a possible physical connection between both galaxies cannot be claimed.

Using `Le PHARE` and fixing the redshift to $z = 0.823$, the SED of the host (Table C.1; including an HST/WFC3 F160W and a *Spitzer*/IRAC1 detection) is best fit by the template of a galaxy with a modest SFR of $\sim1\,M_\odot\,\mathrm{yr}^{-1}$ but a rather high specific SFR of $\log \mathrm{sSFR} \sim -8.6$ (Fig. A.2; Table C.5). These results are in rough agreement with those reported in Vergani et al. (2015).

Details on the SN fitting. When performing the combined afterglow plus SN fit (Eq. (1)) in the r' band, we had to exclude data from 1 to 7 days post-burst. Including these data yields an unrealistic SN component with $k \sim 3.5$ and $s \sim 0.3$, in strong contrast to the values derived in i' and z' (and any known GRB SN). Without these data points, a result in accordance with those in the other photometric bands is derived (Table C.1): The peak luminosity of the SN was ~0.7 times the luminosity of

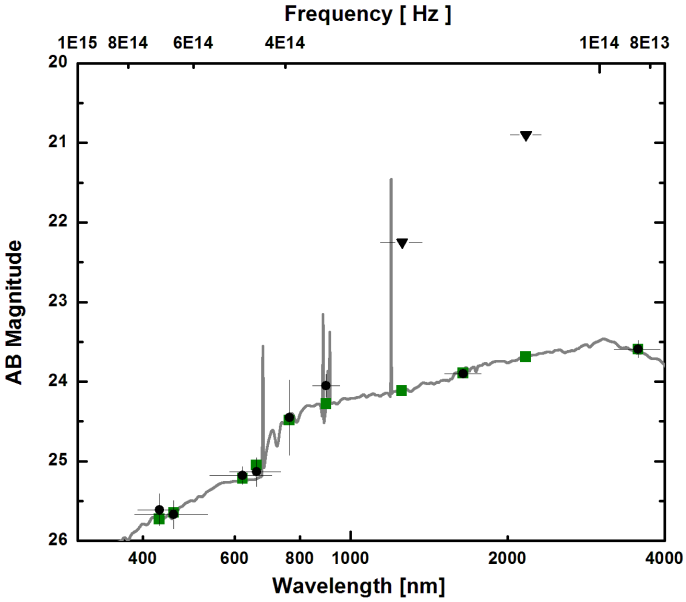

Fig. A.2. SED of the host galaxy of GRB 071112C (corrected for Galactic extinction) based on GROND $g'r'i'$-band data, a GTC z', an HST/F160W (H band), and a *Spitzer*/IRAC1 detection as well as data taken with Keck/LRIS and Gemini-N/GMOS (Table C.11). In JK_s we have only GROND upper limits (Table C.6). The solid line displays the best template fit using `Le PHARE`, green data points are the template-predicted magnitudes. Potential host-galaxy emission lines are indicated.

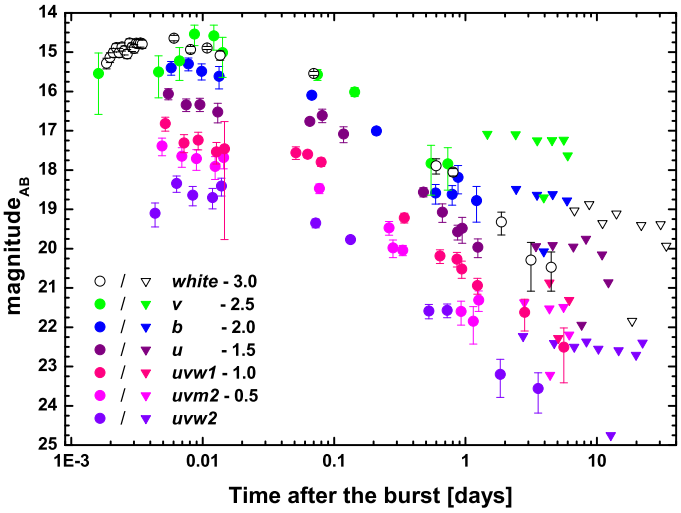

Fig. A.3. UVOT observations of the afterglow of GRB 111228A. Circles with errors are detections and upper limits are downward-pointed triangles. The different bands are offset by steps of 0.5 mag for clarity. Observations yielding upper limits only have also been stacked to produce deeper upper limits, but neither the SN nor the host galaxy are detected at late times.

SN 1998bw, though our measurement error is on the order of 30%. Thereby, the SN developed notably faster than SN 1998bw (stretch factor $s \sim 0.75$). Our results indicate that the GRB SN was similar in terms of evolution and luminosity as GRB/XRF 060218/SN 2006aj and GRB/XRF 100316D/SN 2010bh, that is, fainter and faster than the template SN 1998bw.

A.2. GRB 111228A

The burst and the afterglow data. The burst triggered *Swift*/BAT on 2011 Dec 28 at 15:44:43 UT (Ukwatta et al. 2011). It consisted of multiple spikes and had a duration of $T_{90}(15-350\,\mathrm{keV}) = 101.20 \pm 5.42\,\mathrm{s}$ (Cummings et al. 2011). It was also detected by the *Fermi*/Gamma-ray Burst Monitor (GBM; Meegan et al. 2009) with a duration $T_{90}(50-300\,\mathrm{keV})$ of about 100 s (Briggs & Younes 2011). Its optical afterglow was bright enough to be found by *Swift*/UVOT (Ukwatta et al. 2011). Its spectroscopic redshift is $z = 0.716$ (published values vary between 0.713 and 0.716; Cucchiara & Levan 2011; Dittmann et al. 2011; Palazzi et al. 2011; Schulze et al. 2011; Xu et al. 2011), with the most accurate one coming from X-shooter observations (Schulze et al. 2011). The burst was also detected by Konus-*Wind* (Golenetskii et al. 2011). A possible detection of an SN signal in the light curve of the optical transient 34.5 days after the burst based on TNG imaging data was reported by D'Avanzo et al. (2012). The early optical and X-ray afterglow is studied by Xin et al. (2016) in detail. The authors conclude that the observed early plateau phase of the afterglow light curve suggests an energy injection period provided by a freshly formed magnetar. Since their optical data do not go beyond ~0.3 Ms post-burst, no SN is discussed.

Using GROND, we started observations on Dec 29 at 04:53 UT, 13 h after the trigger (Nicuesa Guelbenzu et al. 2011); additional data were obtained over further 11 epochs, resulting in a good sampling of the optical light curve between about 0.5 and 90 days post burst. This was finalized by a deep host-galaxy observation 4 years later (Table C.7).

We furthermore analyzed the UVOT data for this GRB, stretching from 0.00162 days (140 s) to 33.7 days after the trigger. The afterglow is detected until 5.6 days after the trigger, but neither the SN nor the host galaxy is detected in any filter, even in deep stacks. The UVOT light curves are shown in Fig. A.3 and the data is given in Table C.8.

Afterglow properties. Applying Eq. (1), and using GROND data only, for a joint fit in $g'r'i'z'JHK_s$ and using a broken power-law, we find $\alpha_1 = 1.18 \pm 0.03$, $\alpha_2 = 1.79 \pm 0.05$, $t_\mathrm{b} = 1.68 \pm 0.06$ days. We note that such a break is potentially also apparent in the X-ray light curve (see the *Swift*/X-ray Telescope (XRT) repository, Evans et al. 2007; Xin et al. 2016); however, it would require to skip the very last X-ray data point. The value we found for α_1 agrees with the decay slope reported by Xin et al. (2016), $\alpha = 1.12 \pm 0.10$, though their results are based on a much less well-sampled data base at later times and, therefore, these authors did not find evidence for a break in their optical light curve.

The deduced light-curve parameters do substantially change if early data ($t = 0.02-0.28$ days) from other telescopes (UVOT data and those of Xin et al. 2016) are taken into account. In this case the light curve can still be fitted with a single broken power law, but the pre-break decay slope flattens to $\alpha_1 = 0.06 \pm 0.04$. Such a flat decay suggests an early plateau phase which obviously smoothly developed into a normal afterglow decay phase. When this transition happened is not apparent in the optical/NIR data. Compared to the GROND-only data the break time is at $t_\mathrm{b} = 0.41 \pm 0.07$ days and the post-break decay parameter steepens slightly to $\alpha_2 = 2.00 \pm 0.06$, formally a more comfortable solution as it does not exclude anymore the case $p > 2$.

When only early GROND $g'r'i'z'JHK_s$ data are taken into account, the SED of the afterglow can be described by a power-law without evidence for host extinction ($A_V^\mathrm{host} = 0$ mag). The joint fit of the GROND multi-color data provides a spectral slope of $\beta = 0.88 \pm 0.03$, compared to $\beta \sim 0.75$ as it was deduced by

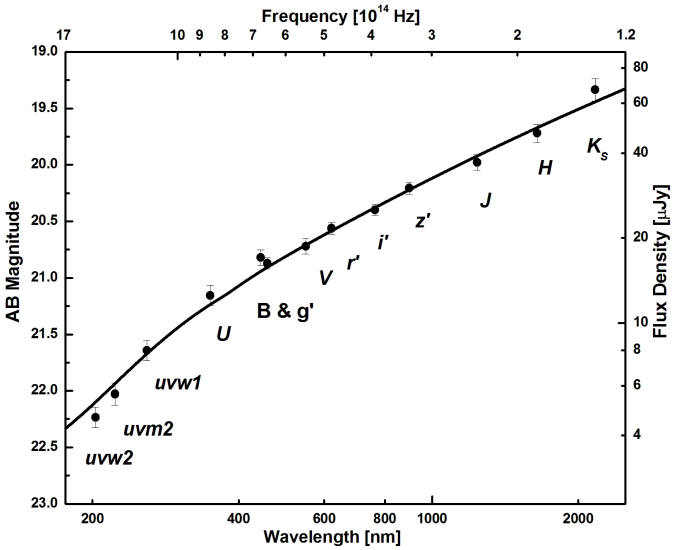

Fig. A.4. SED of the afterglow of GRB 111228A based on GROND as well as *Swift*/UVOT data (Tables C.7, C.8). Magnitudes refer to the time of the light curve break at $t = t_b = 1$ day, i.e., are free of any contribution from an underlying SN component. Data are corrected for Galactic extinction. The SED suggests a host extinction of $A_V^{host} = 0.16$ mag.

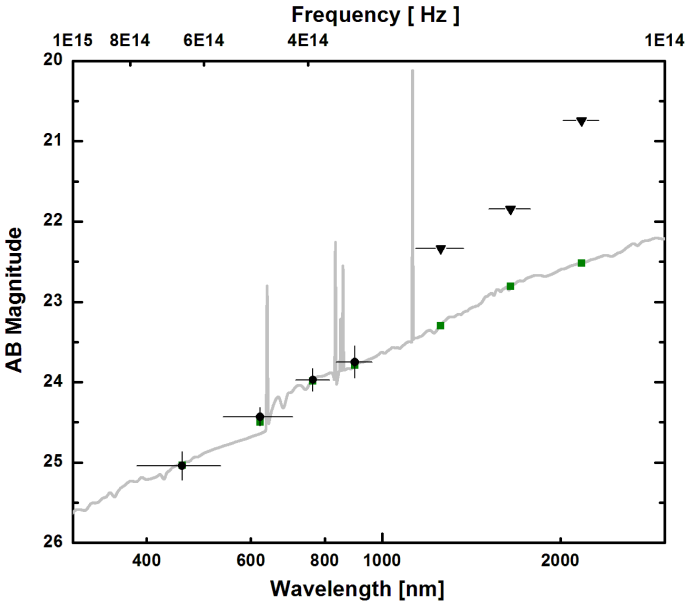

Fig. A.5. SED of the host galaxy of GRB 111228A based on GROND data taken four years after the burst and the corresponding best galaxy-template SED found by `Le PHARE` (for the color coding see Fig. A.2). Due to the lack of a NIR detection, the fit is rather ill-defined.

Xin et al. (2016). Taking into account *Swift*/UVOT data, such a fit however shows a deficit of flux in the UV domain, which can be attributed to 0.16 mag of host-galaxy visual extinction (adopting an SMC extinction law). This changes the spectral slope of the afterglow to $\beta = 0.69 \pm 0.07$ (Fig. A.4), in agreement with Xin et al. (2016).

Neither the GROND-only light-curve parameters (which imply $p < 2$) nor the light-curve parameters based on the extended data set (which suggest $p > 2$) lead to a reasonable solution for the α–β relations (Table C.3). Interpreting the (GROND-only) light curve break at $t = 1.68$ days as a jet break, and using the observed isotropic equivalent energy (Table 1), this implies a jet half-opening angle of $\Theta_{ISM} = 6.3 \pm 0.1$ deg for an ISM and $\Theta_{wind} = 5.4 \pm 0.1$ deg for a wind model, and a beaming-corrected energy release (erg) of $\log E_{corr,ISM}[erg] = 50.39 \pm 0.04$ and $\log E_{corr,wind}[erg] = 50.26 \pm 0.03$, respectively.

Host galaxy properties. We detect a galaxy at the location of the GRB in $g'r'i'z'$ in our last-epoch GROND images taken 1499 days post burst (Fig. A.5, Table C.1). On a GROND white-band image the SN is located $0\farcs28 \pm 0\farcs20$ east of the brightness center of its host (2.1 ± 1.5 kpc). Using `Le PHARE` and fixing the redshift to $z = 0.716$, the SED of the host (Table C.1) suggests a dusty galaxy ($E(B-V) = 0.4$ mag). Its SFR, mass, and specific SFR are similar to those of the host of GRB 071112C (Fig. A.5; Table C.5).

Details on the SN fitting. The GROND $r'i'$ light curves show a slight but clearly visible bump around $t = 20$ days (Fig. 1). It is also marginally seen in z' but not apparent in the g' band. When performing the joint fit, we therefore fixed $k_{g'} = 0$, that is, we assumed that there was no contribution from SN light in this photometric band (centered at a wavelength of 2650 Å in the rest frame). Leaving this k-value as a free parameter did otherwise worsen the fit and finally, within the errors, included a solution with $k = 0$. In doing so, for the SN parameters we obtained k values rather typical for most GRB SNe. The stretch factor however is relatively large, $s \sim 1.2$–1.6, implying that this SN evolved slower than SN 1998bw (Table C.1). We note, however, that due to the relatively weak SN bump the deduced SN peak time is rather sensitive to the light curve fit at early times. The error for s is, as always, the pure mathematical error of the fit but does not take into account this problem. Therefore, the rather large stretch factor deduced for this event should be taken with care.

A.3. GRB 120714B

The burst and the afterglow data. The burst was detected by *Swift*/BAT on 2012 July 14 at 21:18:47 UT (Saxton et al. 2012). It is dominated by a broad peak with a duration $T_{90}(15\text{–}350\,keV) = 159 \pm 34$ s (Cummings et al. 2012). The optical afterglow was discovered by *Swift*/UVOT (Marshall & Saxton 2012). Its spectroscopic redshift was soon found to be $z = 0.3984$ (Fynbo et al. 2012b), suggesting that an upcoming SN component might be detectable. Given the redshift, the observed relatively low mean luminosity of the burst (Table C.2) defines it as a member of the class of intermediate-luminosity GRBs (Schulze et al. 2014).

Using GROND, we started observing about 6 h after the burst (Nicuesa Guelbenzu et al. 2012), though weather conditions were inclement at that time (airmass > 2.2, mean seeing 2″.4). Because of the very-well-detectable SN component in the light curve of the optical transient (Klose et al. 2012a,b), GROND observed the field for altogether 17 epochs up to 449 days post burst (Table C.9).

Afterglow properties. Since no SN is apparent in the g' band, we used this band to measure the decay slope of the optical transient (Table C.2). Moreover, since no evidence for a break is detectable in the g'-band light curve, we adopted a single power-law decay and find $\alpha = 0.58 \pm 0.06$. Only a lower limit on the time of a potential jet break can be set: of $t_b \gtrsim 10$ days. No *Swift*/X-ray light-curve data are available to support this conclusion further.

Adopting a break time of $t_b > 10$ day, and using the observed isotropic equivalent energy (Table 1), this gives for the jet half-opening angle $\Theta_{ISM} > 9.5 \pm 0.3$ deg for an ISM and $\Theta_{wind} >$

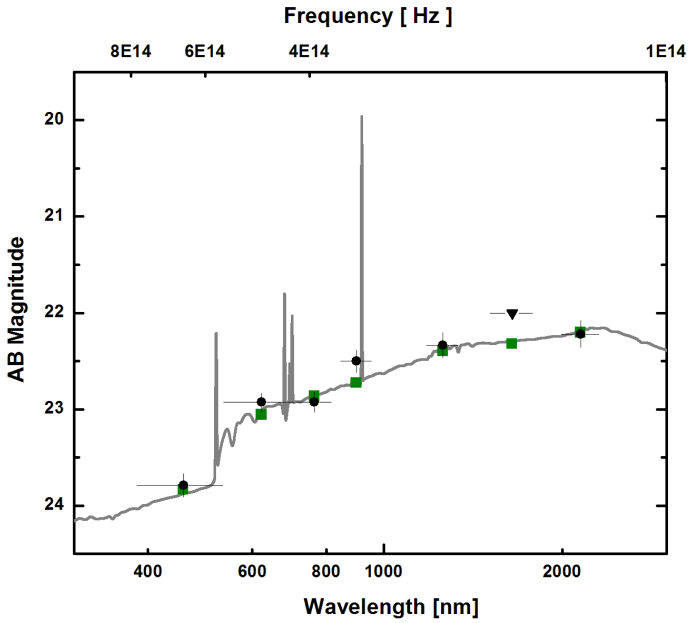

Fig. A.6. SED of the host galaxy of GRB 120714B based on GROND $g'r'i'z'H$ and HAWKI JK_s-band data. The SED is best described by a galaxy undergoing an episode of intense star-forming activity (for the color coding see Fig. A.2).

14.5 ± 1.0 deg for a wind model. The corresponding upper limits for the beaming-corrected energy release (erg) are log $E_{\rm corr,ISM}$[erg] > 48.90 ± 0.09 and log $E_{\rm corr,wind}$[erg] > 49.26 ± 0.06, respectively.

As we discussed in Sect. 3.3, our X-shooter spectroscopy revealed that the early first-epoch GROND data are affected by an additional radiation component. Taking this into account provides for the afterglow light a spectral slope of $\beta = 0.7 \pm 0.4$. Better constraints on β can not be obtained, already at day two the rapid rise of the SN component and the comparably rather bright host galaxy prevent a reliable measurement of the afterglow SED. Using the α–β relations no model is really ruled out (Table C.3).

Host galaxy properties. In order to detect the GRB host galaxy, GROND observed the field again 449 days post-burst. In addition, we obtained HAWKI J and K_s-band images on Oct 13, 2013, one year after the SN maximum (Program ID: 092.A-0231, PI: T. Krühler).

Stacking the GROND $g'r'i'z'$-band images into a white-band frame reveals that the SN was located 0.″21 ± 0.″20 (1.2 ± 1.1 kpc) east of the center of its host (Fig. 14). The SED of the host is well-determined, with detections in $g'r'i'z'$ by GROND and JK_s with HAWKI. Using `Le PHARE`, and fixing the redshift to $z = 0.3984$, the best template to describe the SED (Table C.1) is a dusty ($E(B-V) \sim 0.3$ mag) galaxy with a rather modest SFR of about 1 $M_\odot$ yr^{-1}. Its mass in stars and specific SFR resemble the properties of the host of GRB 071112C (Fig. A.6; Table C.5).

Details on the SN fitting. In the $r'i'z'$-band light curves a SN bump is clearly seen, while no SN signal is evident in the g'-band data (centered at a wavelength of 3250 Å in the rest frame; Fig. 1). This lack of SN flux at shorter wavelengths is also evident in our SN spectrum (Sect. 3.2). Such a strong damping in the host-UV band is reminiscent of the otherwise more luminous SN 2009nz associated with GRB 091127 (Olivares et al. 2015; Kann et al. 2016). When performing the joint fit in order to obtain the SN (k, s) values, for the g' band we fixed $k = 0$. In doing so, we find that in $r'i'z'$ (corresponding to wavelengths of about 4480–6390 Å in the GRB rest frame) the SN reached between about 50–80% of the peak luminosity of SN 1998bw, while in i' and z' it evolved about 10% faster (Table C.1). Compared to GRB SNe that have been analyzed with the (k, s) methodology (Zeh et al. 2004; Ferrero et al. 2006; Thöne et al. 2011; Cano 2013), SN 2012eb is among the faintest GRB SNe detected so far. Especially, it is markedly fainter than GRB 120422A/SN 2012bz which is, analogous to GRB 120714B, another intermediate-luminosity GRB (Schulze et al. 2014, but see Cano et al. 2017).

A.4. GRB 130831A

The burst and the afterglow data. GRB 130831A was detected by *Swift*/BAT on 2013 Aug 31 at 13:04:16 UT Hagen et al. (2013). It is dominated by a FRED-like profile followed by additional emission. Its duration was T_{90}(15−350 keV) = 32.5 ± 2.5 s (Barthelmy et al. 2013). The optical afterglow was discovered by *Swift*/UVOT (Hagen et al. 2013). A redshift $z = 0.4791$ was soon reported by Cucchiara & Perley (2013) based on observations with Gemini-North. The GRB was also detected by Konus-*Wind* at 13:04:22 UT and an isotropic energy release of $E_{\rm iso} = (4.6 \pm 0.2) \times 10^{51}$ erg was determined (Golenetskii et al. 2013).

The first follow-up observations with GROND started at 03:33 UT (14.5 h after the burst) and continued for 3.3 h. Further data were obtained until 33.6 days after the burst, and a final host-galaxy observation was obtained 387 days after the GRB (in total 12 epochs, Table C.10). Observations were constrained by a relatively narrow visibility window and affected by permanently high airmass (1.9 at best). No GROND data could be obtained around the peak time of the GRB SN.

Afterglow properties. The early optical afterglow light curve (at $t \lesssim 5$ ks) is complex and variable, and is discussed in detail in De Pasquale et al. (2016). We did not use these data for the calculation of the light curve parameters. Since there is no evidence for a break in the optical light curve, we adopted a single power-law decay, which provides $\alpha = 1.61 \pm 0.01$ and a spectral slope $\beta = 1.00 \pm 0.05$ (Fig. 1), suggesting a post-break evolutionary phase. When compared with the afterglow sample of Zeh et al. (2006) its interpretation as a pre-break decay slope is however not excluded. For example, the afterglow of GRB 000926 had $\alpha_1 = 1.74 \pm 0.03$, $\alpha_2 = 2.45 \pm 0.05$.

In order to characterize the underlying SN component, we combined our data with that of Cano et al. (2014), De Pasquale et al. (2016), and Khorunzhev et al. (2013). To avoid the early complex light-curve evolution, we only used data from 0.39 days onward. We fitted the $g'r'R_{\rm c}i'I_{\rm c}z'$-band data using a simple power law, sharing the decay slope (we find no evidence for any chromatic evolution). The SN parameters k and s were left as free parameters, individual in each band, as is the host galaxy magnitude. We also tried a fit with the afterglow described by a broken power law, but found that the break time and post-break decay slope are unconstrained, while at the same time the k, s parameters hardly changed. Therefore, there is no evidence in the afterglow of a break between 0.4 and ∼3 days, in agreement with the lack of a break in the late X-ray light curve (De Pasquale et al. 2016).

The SED of the optical/NIR afterglow is well-fit by a power law (Fig. A.7). There is no evidence for host-galaxy extinction along the line of sight, in agreement with Cano et al. (2014) and De Pasquale et al. (2016). The α–β relations suggest that the deduced afterglow parameters rule out a jet model with

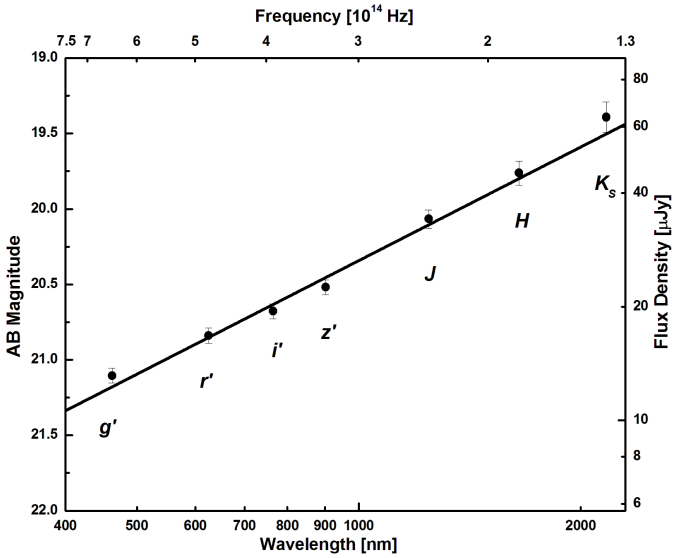

Fig. A.7. GROND ($g'r'i'z'JHK_s$) SED of the afterglow of GRB 130831A. Magnitudes refer to $t = 1$ day (corrected for Galactic extinction). There is no evidence for host-galaxy extinction.

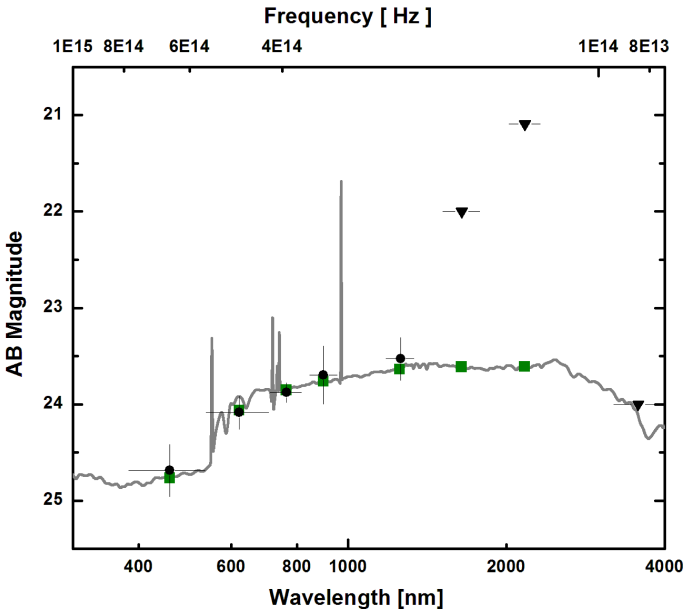

Fig. A.8. SED of the host galaxy of GRB 130831A (the color coding follows Fig. A.2).

$\nu_{\rm obs} < \nu_{\rm c}$ but exclude neither a jet model with $\nu_{\rm obs} > \nu_{\rm c}$ nor a spherical wind/ISM model (Table C.3). If the jet-break time was at $t_{\rm b} > 1$ day then the observed isotropic-equivalent energy release (Table 1), implies a jet half-opening angle of $\Theta_{\rm ISM} > 6.8 \pm 0.1$ deg and a beaming-corrected energy (erg) of log $E_{\rm corr,ISM}$[erg] $> 49.70 \pm 0.03$. For a wind model these numbers are $\Theta_{\rm wind}$[erg] $> 7.6 \pm 0.2$ deg and log $E_{\rm corr,wind} > 49.80 \pm 0.02$.

Nevertheless, a very early jet break cannot be ruled out. A potential example for such a case is GRB 061007, which was exceptionally bright across the electromagnetic spectrum and whose afterglow showed a remarkably similar temporal decay slope of $\alpha = 1.65 \pm 0.01$ from early-on (Schady et al. 2007). It has been argued by Schady et al. (2007) that here the scenario of a very narrow jet ($\Theta < 0.8$ deg) can fit the observational data well.

We finally note that De Pasquale et al. (2016) and Zhang et al. (2016) proposed that the early X-ray and optical data of the afterglow suggest a continuous energy input from a magnetar. Our data cannot be used to evaluate this model further.

Host galaxy properties. We used the late-epoch GROND $g'r'z'$-band detections of the host galaxy one year after the burst together with the results of our joint light-curve fit for the i' band (Fig. A.8), as well as a J-band detection by Keck/MOSFIRE and a deep 3.6μm upper limit from *Spitzer*/IRAC (Table C.11) to construct the SED (Table C.1). Applying `Le PHARE`, and fixing the redshift to $z = 0.4791$, the best template is a dusty galaxy ($E(B-V) = 0.2$ mag) with a rather low SFR on the order of 0.3 $M_\odot$ yr^{-1}. Its mass and specific SFR are, within errors, rather normal for long-GRB hosts (Table C.5).

Using the GROND $g'r'$ combined image, we find that the SN was located $0\farcs92 \pm 0\farcs20$ (projected distance 5.3 ± 1.2 kpc) east of the center of its host galaxy (Fig. 14).

Details on the SN fitting. Due to some scatter in the data, the joint fit is formally bad (Table C.1), but the SN is well-sampled in all GROND optical bands. The steep afterglow decay slope ($\alpha = 1.61 \pm 0.01$) is in agreement with the one derived by Cano et al. (2014) and De Pasquale et al. (2016). As we do not find any evidence for rest-frame extinction, the k values derived directly from the fit for the individual bands are not further corrected for host-galaxy extinction (Table C.1). In general,

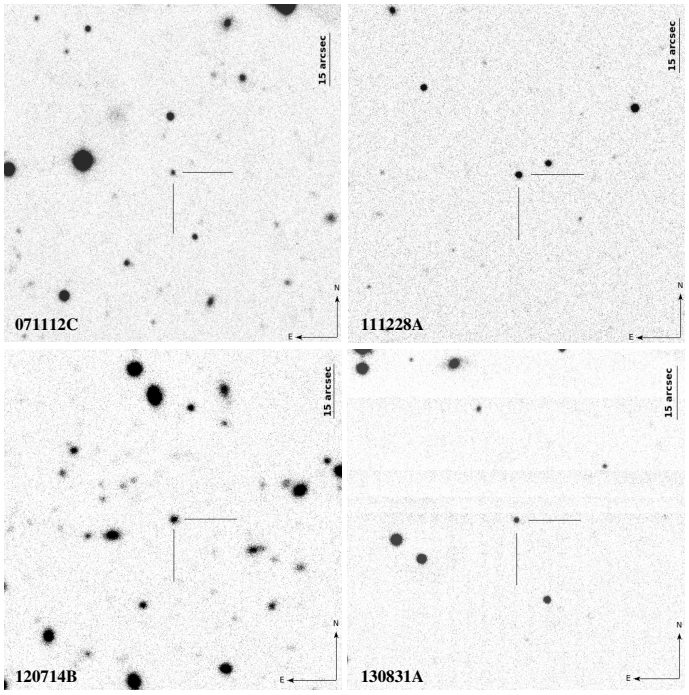

Fig. A.9. Finding charts of the GRB fields. Shown here are the afterglows as imaged by GROND in the r' band. *Top left panel*: 0.369 days after the burst, *top right panel*: 0.648 days, *bottom left panel*: 0.396 days, *bottom right panel*: 0.689 days.

we find that SN 2013fu evolves faster than SN 1998bw ($s \sim 0.6$ to 0.8) and is somewhat less luminous ($k \sim 0.6$ to 1.0), though it shows signs of being photometrically different. It was significantly fainter than SN 1998bw in r' and z' while of similar luminosity in g' and i'. These values are in agreement with those derived by Cano et al. (2014), with the exception of the z' band, where our data point to a significantly fainter SN. Cano et al. (2014) have only a single data point during the SN phase in z', and this value is not host-subtracted either, we therefore believe our derived value to be more trustworthy.

Appendix B: Details of Fig. 13

The data sources for the light curve of the afterglow of GRB 071112C are given in Kann et al. (2010). In addition, we added the data presented in this work. We shifted data from other bands to the r' band, subtracted the host-galaxy contribution, and only data up to six days were considered. We used the data presented in this paper as well as the data set of Xin et al. (2016) to construct a compound light curve of the afterglow of GRB 111228A. Here, we used late-time data in the g' band, for which we were unable to discern a SN component, host-corrected and shifted them to the r' band. We also used this method to derive the compound light curve of the afterglow of GRB 120714B. At early times, we used two UVOT white-filter detections[18], and in doing so we assumed white = R_c in Vega magnitudes. The host-subtracted light curve is well-described by a single power-law decay over its entire timespan. The extremely well-time-resolved light curve of the afterglow of GRB 130831A was constructed from our data as well as the extensive data sets of De Pasquale et al. (2016), Cano et al. (2014), and Gorbovskoy et al. (2015). In this case, the associated SN 2013fu is also detected in the g' band, and therefore we used the analytical results from our fit to subtract the SN component and extend the pure afterglow light curve.

We extended the sample by adding light curves for further GRB SNe studied by Kann et al. (2016). The data of XRF 020903 were host-subtracted already, and we only extend the light curve to six days post-burst. In the case of GRB 120729A, the afterglow and the SN are well-separated (the afterglow breaks early and decays steeply), so only data until 0.8 days were taken into account. For GRB 130215A, the SN is only detected at low significance and we cut the light curve off at 17 days; no host is detected in this case. In the cases of GRBs 130702A and 140606B, we subtracted both the individual host-galaxy magnitudes as well as the SN contributions from the r' and i' light curves, then merged them according to the colors derived from the respective SEDs.

Kann et al. (2006) labeled the shift in magnitude dR_c. For the GRBs in this paper, we find: GRB 111228A: $dR_c = +0.62^{+0.06}_{-0.07}$ mag; GRB 120714B: $dR_c = +2.17^{+0.05}_{-0.06}$ mag; GRB 130831A: $dR_c = +1.97^{+0.01}_{-0.02}$ mag; the value for GRB 071112C is taken from Kann et al. (2010).

Appendix C: Summarizing tables and log of the observations

Table C.1. Summary of the measured supernova parameters.

GRB	071112C	111228A	120714B	130831A
$k_{g'}$	...	...	...	0.87 ± 0.24
$k_{r'}$	0.53 ± 0.17	0.63 ± 0.14	0.47 ± 0.05	0.61 ± 0.04
$k_{i'}$	0.70 ± 0.17	0.73 ± 0.15	0.74 ± 0.06	0.99 ± 0.05
$k_{z'}$	0.52 ± 0.21	0.85 ± 0.27	0.78 ± 0.08	0.58 ± 0.12
$s_{g'}$	...	...	...	0.64 ± 0.09
$s_{r'}$	0.75 ± 0.19	1.58 ± 0.23	0.66 ± 0.04	0.80 ± 0.02
$s_{i'}$	0.78 ± 0.23	1.20 ± 0.25	0.91 ± 0.06	0.72 ± 0.02
$s_{z'}$	0.71 ± 0.35	1.45 ± 0.25	0.95 ± 0.09	0.72 ± 0.07
$t_{g',\mathrm{obs},p}$ (days)	...	...	...	13.7 ± 2.5
$t_{r',\mathrm{obs},p}$	23.1 ± 6.6	45.8 ± 9.1	15.6 ± 2.3	20.0 ± 2.8
$t_{i',\mathrm{obs},p}$	26.2 ± 8.7	37.9 ± 9.8	23.4 ± 4.9	19.6 ± 3.0
$t_{z',\mathrm{obs},p}$	24.7 ± 12.8	47.5 ± 11.3	25.4 ± 5.9	20.3 ± 3.8
$t_{g',\mathrm{obs},p}$	...	...	...	9.3 ± 1.7
$t_{r',\mathrm{obs},p}$	12.7 ± 3.6	26.7 ± 5.3	11.2 ± 1.7	13.5 ± 1.9
$t_{i',\mathrm{obs},p}$	14.4 ± 4.8	22.1 ± 5.7	16.7 ± 2.8	13.2 ± 2.0
$t_{z',\mathrm{obs},p}$	13.6 ± 7.0	27.7 ± 6.6	18.1 ± 3.4	13.8 ± 2.6
$\log L_{\mathrm{bol}}$ (erg s^{-1})	42.73 ± 0.08	42.83 ± 0.09	42.79 ± 0.05	42.84 ± 0.05
t_p (days)	11.9 ± 2.4	22.7 ± 2.2	13.6 ± 0.7	11.9 ± 0.3
$v_{\mathrm{exp;obs}}$ (km s^{-1})	...	...	43 000 ± 5300	20 400 ± 3500
$v_{\mathrm{exp;peak}}$	...	...	42 000 ± 5500	30 300 ± 6000

Notes. The first eight rows summarize the measured (s, k) values in the GROND $g'r'i'z'$ bands. The following rows contain the corresponding SN peak times in the observer as well as in the host galaxy frame, $t_p(\mathrm{SN}) = t_p(\mathrm{SN\ 1998bw}) \times s$. Thereby we used the light-curve peak times for SN 1998bw as they follow from our SN fitting procedure (Zeh et al. 2004): $t_p(g') = 14.5 \pm 1.7$, $t_p(r') = 16.9 \pm 2.3$, $t_p(i') = 18.4 \pm 2.8$, $t_p(z') = 19.1 \pm 3.1$ days. The following two rows provide the bolometric luminosity, $L_{\mathrm{bol}} = k_{\mathrm{bol}}\, L^{\mathrm{bw}}_{\mathrm{bol}}$, as well as the bolometric light-curve peak time (given by $t_p^{\mathrm{bw}} \times s_{\mathrm{bol}}$, with $t_p^{\mathrm{bw}} = 15.86 \pm 0.18$ days; Prentice et al. 2016). The two last rows list the photospheric expansion velocity as it was measured and its calculated value for the time of the peak of the bolometric light curve.

[18] http://swift.gsfc.nasa.gov/uvot_tdrss/526642/index.html

Table C.2. Summary of the afterglow light-curve fits.

	GRB	071112C	111228A	120714B	130831A
Afterglow	RA (J2000)	02:36:50.955	10:00:16.032	23:41:38.076	23:54:29.882
	Dec. (J2000)	+28:22:16.70	+18:17:51.94	−46:11:01.72	+29:25:46.11
	α_1	0.96 ± 0.01	1.18 ± 0.03	0.58 ± 0.06	1.61 ± 0.01
	α_2	...	1.79 ± 0.05	...	...
	t_b (days)	...	1.68 ± 0.06	...	...
	n	...	10	...	...
	χ^2/d.o.f.	1.08	0.78	0.87	2.50
Afterglow SED	g' (corr. mag)	22.80 ± 0.08	20.87 ± 0.05	...	21.11 ± 0.05
	r'	22.69 ± 0.08	20.56 ± 0.05	...	20.84 ± 0.05
	i'	22.62 ± 0.09	20.40 ± 0.05	...	20.68 ± 0.05
	z'	22.56 ± 0.09	20.21 ± 0.05	...	20.52 ± 0.05
	J	22.33 ± 0.12	19.98 ± 0.07	...	20.07 ± 0.06
	H	22.05 ± 0.26	19.72 ± 0.08	...	19.76 ± 0.08
	K_s	21.95 ± 0.35	19.33 ± 0.10	...	19.39 ± 0.10
	$E_{(B-V),\mathrm{Gal}}$ (mag)	0.12	0.03	0.01	0.04
	β_{obs}	0.44 ± 0.11	0.69 ± 0.07	0.7 ± 0.4	1.00 ± 0.05
	A_V^{host} (mag)	0	0.16 ± 0.04	0	0
	χ^2/d.o.f.	0.23	0.86	6.5	0.66

Notes. The afterglow magnitudes forming the SEDs are corrected for the Galactic reddening, $E_{(B-V),\mathrm{Gal}}$, along the line of sight. In the case of GRB 120714B the afterglow SED was only roughly determined based on VLT/X-shooter data taken 0.353 days after the burst (see Sect. 3.3). In this case, for the SN light curve fits $A_V^{\mathrm{host}} = 0$ mag is assumed, not measured. In order to be consistent with the host-galaxy measurements (see Table C.4), in the case of GRB 130831A afterglow coordinates were measured on the VLT acquisition images. Otherwise GROND images were used.

Table C.3. Summary of the α–β relations.

Model/GRB	071112C	111228A	120714B	130831A
	$\beta_{\mathrm{obs}} = 0.44 \pm 0.11$	$\beta_{\mathrm{obs}} = 0.69 \pm 0.07$	$\beta_{\mathrm{obs}} = 0.7 \pm 0.4$	$\beta_{\mathrm{obs}} = 1.00 \pm 0.05$
	β_{theo}	$\beta_{\mathrm{theo}}(p > 2), \beta_{\mathrm{theo}}(p < 2)$	β_{theo}	β_{theo}
ISM, iso, $\nu < \nu_c$	0.64 ± 0.01	0.04 ± 0.03, 1.65 ± 0.08	0.39 ± 0.04	1.07 ± 0.01
ISM, iso, $\nu > \nu_c$	0.97 ± 0.01	0.37 ± 0.03, 1.48 ± 0.08	0.72 ± 0.04	1.41 ± 0.01
wind, iso, $\nu < \nu_c$	0.31 ± 0.01	−0.29 ± 0.03, 0.22 ± 0.12	0.05 ± 0.04	0.74 ± 0.01
wind, iso, $\nu > \nu_c$	0.97 ± 0.01	0.37 ± 0.03, 1.72 ± 0.12	0.72 ± 0.04	1.41 ± 0.01
ISM, jet, $\nu < \nu_c$	–	0.50 ± 0.03, 0.08 ± 0.10	–	0.31 ± 0.01
ISM, jet, $\nu > \nu_c$	–	1.00 ± 0.03, 0.58 ± 0.10	–	0.81 ± 0.01
wind, jet, $\nu < \nu_c$	–	0.50 ± 0.03, 0.08 ± 0.10	–	0.31 ± 0.01
wind, jet, $\nu > \nu_c$	–	1.00 ± 0.03, 0.58 ± 0.10	–	0.81 ± 0.01

Notes. Predicted spectral slope β_{theo} for the afterglows adopting for the power-law index p of the electron distribution function a value $p > 2$ (GRB 071112C, 111228A, 120714B, 130831A) or $p < 2$ (GRB 111228A; Zhang & Mészáros 2004). Values for α_1 and α_2 are taken from Table C.2. Individual events: GRB 071112C: the observed decay slope α implies that the afterglow is in the spherical expansion phase. GRB 111228A: shown here are the results for the extended data set (which suggests $p > 2$) and for the GROND-only data (which imply $p < 2$). GRB 120714B: the observed decay slope α implies that the afterglow is in the spherical expansion phase. GRB 130831A: the observed decay slope could either be pre- or post-break. Therefore, both options are calculated.

Table C.4. Summary of the host-galaxy data.

GRB	071112C	111228A	120714B	130831A
RA (J2000)	02:36:50.965	10:00:16.051	23:41:38.057	23:54:29.831
Dec	+28:22:16.48	+18:17:52.01	−46:11:01.64	+29:25:45.73
g'	25.67 ± 0.06	25.04 ± 0.17	23.80 ± 0.13	24.69 ± 0.27
r'	25.18 ± 0.11	24.44 ± 0.12	22.93 ± 0.10	24.08 ± 0.17
i'	24.45 ± 0.47	23.98 ± 0.14	22.70 ± 0.10	23.88 ± 0.10
z'	24.05 ± 0.14	23.75 ± 0.20	22.50 ± 0.12	23.69 ± 0.30
J	>22.3	>22.3	22.34 ± 0.13	23.49 ± 0.22
H	23.91 ± 0.06	>21.8	>21.8	>22.0
K_s	>21.0	>20.7	22.22 ± 0.14	>21.1
Offset SN	0.″26 ± 0.″20	0.″28 ± 0.″20	0.″21 ± 0.″20	0.″92 ± 0.″20
Offset SN (kpc)	2.1 ± 1.6	2.1 ± 1.5	1.2 ± 1.1	5.3 ± 1.2

Notes. Magnitudes are given in the AB system and corrected for Galactic extinction according to Schlafly & Finkbeiner (2011). Notes on individual objects: GRB 071112C: z' and H-band magnitudes were taken from Vergani et al. (2015; the near-infrared band data point is actually based on an observation with the HST F160W filter), g'- and r'-band magnitudes are based on Gemini-North/GMOS observations. GRB 120714B: JK_s-band magnitudes stem from our VLT/HAWKI observations. GRB 130831A: the J-band magnitude is based on Keck/MOSFIRE observations (Table C.11), the i'-band magnitude was derived based on our light-curve fit. See Table C.11 for additional host-galaxy detections and upper limits in other filters. All other magnitudes are based on late-epoch observations with GROND. In the case of GRB 130831A the host-galaxy coordinates were measured on the VLT acquisition images, otherwise GROND images were used.

Table C.5. Results of the stellar population synthesis fits using `Le PHARE` and adopting a starburst model.

GRB	M_B (mag)	$E(B-V)_{host}$ (mag)	log SFR ($M_\odot$ yr^{-1})	log $M/M_\odot$	log sSFR (yr^{-1})	χ^2
071112C	−18.49	0.15	$0.22^{+0.60}_{-0.44}$	$8.67^{+0.16}_{-0.23}$	$-8.44^{+0.86}_{-0.61}$	2.11
111228A	−18.57	0.40	$0.33^{+0.63}_{-0.61}$	$8.72^{+0.24}_{-0.24}$	$-8.41^{+0.68}_{-0.65}$	0.01
120714B	−18.33	0.08	$-0.32^{+0.42}_{-0.29}$	$8.72^{+0.16}_{-0.17}$	$-9.06^{+0.58}_{-0.38}$	0.01
130831A	−17.72	0.02	$-0.25^{+0.75}_{-0.56}$	$8.43^{+0.47}_{-0.32}$	$-8.66^{+0.82}_{-0.83}$	0.55
Median values of the unbiased *Swift*/BAT6 GRB host galaxy sample at $z < 1$ from Vergani et al. (2015)						
	...	$0.00^{+0.08}_{-0.00}$	$-0.07^{+0.59}_{-0.30}$	$8.84^{+0.25}_{-0.60}$	$-8.72^{+0.31}_{-0.26}$	...
Median values of the $z < 0.5$ GRB host galaxy sample from Schulze et al. (2018)						
	−18.33 ± 0.41	...	−0.19 ± 0.13	8.83 ± 0.20	−9.15 ± 0.11	...

Notes. The integrated host properties were derived by fitting the SED of the host galaxies with stellar-population-synthesis models by Bruzual & Charlot (2003) in `Le PHARE`. The SEDs of the BAT6 sub-sample were fitted using the same method. The errors of the median values indicate the distance to the 16 and 84%-iles.

Table C.6. GRB 071112C: GROND AB magnitudes and upper limits of the optical transient.

$t - t_0$	g'	r'	i'	z'	J	H	K_s
0.322	22.54 ± 0.14	22.20 ± 0.08	21.95 ± 0.16	21.84 ± 0.24	–	–	–
0.330	22.63 ± 0.06	22.21 ± 0.06	21.97 ± 0.11	21.88 ± 0.16	–	–	–
0.347	22.57 ± 0.03	22.31 ± 0.03	22.13 ± 0.06	21.89 ± 0.07	–	–	–
0.369	22.64 ± 0.03	22.44 ± 0.04	22.17 ± 0.06	22.08 ± 0.10	–	–	–
0.392	22.72 ± 0.03	22.44 ± 0.03	22.30 ± 0.05	22.13 ± 0.08	21.66 ± 0.13	21.44 ± 0.26	21.31 ± 0.35
0.415	22.73 ± 0.03	22.49 ± 0.03	22.33 ± 0.06	22.07 ± 0.07	–	–	–
0.438	22.76 ± 0.03	22.48 ± 0.04	22.32 ± 0.07	22.17 ± 0.08	–	–	–
0.454	22.80 ± 0.11	22.55 ± 0.08	22.30 ± 0.11	22.16 ± 0.18	–	–	–
1.392	23.90 ± 0.04	23.63 ± 0.06	23.34 ± 0.07	23.24 ± 0.14	>22.35	>21.82	>21.02
2.402	24.73 ± 0.10	24.05 ± 0.10	23.79 ± 0.14	23.65 ± 0.23	>22.34	>21.62	>20.93
3.387	25.20 ± 0.27	24.48 ± 0.18	23.77 ± 0.21	>23.53	>22.30	>21.30	>20.94
6.409	25.05 ± 0.40	24.33 ± 0.22	24.28 ± 0.29	>24.05	>22.17	>21.46	>20.70
8.365	>24.23	>24.30	24.38 ± 0.47	23.82 ± 0.35	>22.17	>21.32	>20.58
14.369	>24.46	24.36 ± 0.31	>24.01	>23.69	>21.88	>21.09	>20.73
17.343	25.50 ± 0.23	24.73 ± 0.13	24.07 ± 0.20	23.54 ± 0.21	>22.24	>21.32	>20.51
21.357	>25.36	24.72 ± 0.24	23.91 ± 0.18	23.45 ± 0.25	>22.11	>21.35	>20.29
22.317	>25.61	25.03 ± 0.46	23.85 ± 0.19	23.76 ± 0.33	>22.20	>21.30	>20.78
24.327	25.58 ± 0.31	24.63 ± 0.19	24.22 ± 0.23	24.03 ± 0.38	>22.35	>21.51	>20.86
28.333	25.49 ± 0.25	25.05 ± 0.22	24.33 ± 0.26	23.72 ± 0.25	>22.14	>21.55	>20.74
2534.453	25.51 ± 0.43	25.13 ± 0.28	24.69 ± 0.47	>23.68	>21.90	>21.37	>20.54

Notes. $t - t_0$ is the time in units of days after the burst (t_0 = 12 November 2007, 18:32:57 UT; Perri et al. 2007). The data are not corrected for Galactic extinction.

Table C.7. GRB 111228A: GROND AB magnitudes and upper limits of the optical transient.

$t - t_0$	g'	r'	i'	z'	J	H	K_s
0.552	–	19.80 ± 0.02	–	–	–	–	–
0.556	20.09 ± 0.02	19.81 ± 0.02	19.59 ± 0.03	19.54 ± 0.052	19.27 ± 0.12	19.32 ± 0.23	18.55 ± 0.21
0.561	20.09 ± 0.02	19.81 ± 0.01	19.63 ± 0.03	19.45 ± 0.045	19.14 ± 0.10	18.63 ± 0.10	18.49 ± 0.22
0.568	20.15 ± 0.02	19.82 ± 0.01	19.63 ± 0.02	19.40 ± 0.023	19.23 ± 0.06	18.84 ± 0.07	18.84 ± 0.22
0.577	–	19.85 ± 0.01	19.70 ± 0.02	19.43 ± 0.027	19.19 ± 0.05	18.93 ± 0.07	18.64 ± 0.20
0.586	20.20 ± 0.01	19.86 ± 0.01	19.67 ± 0.02	19.46 ± 0.020	19.15 ± 0.06	18.88 ± 0.07	18.54 ± 0.15
0.595	20.20 ± 0.02	19.89 ± 0.01	19.70 ± 0.02	19.47 ± 0.019	19.21 ± 0.05	19.28 ± 0.09	18.76 ± 0.16
0.604	–	19.91 ± 0.01	19.70 ± 0.02	19.49 ± 0.022	19.19 ± 0.05	18.96 ± 0.07	18.60 ± 0.16
0.613	20.23 ± 0.01	19.92 ± 0.01	19.72 ± 0.02	19.51 ± 0.022	19.23 ± 0.06	19.05 ± 0.08	19.00 ± 0.21
0.622	20.25 ± 0.01	19.92 ± 0.01	19.73 ± 0.01	19.52 ± 0.022	19.21 ± 0.06	18.94 ± 0.07	18.55 ± 0.14
0.631	20.28 ± 0.01	19.95 ± 0.01	19.77 ± 0.02	19.56 ± 0.023	19.25 ± 0.06	19.08 ± 0.09	18.60 ± 0.14
0.640	20.28 ± 0.01	19.98 ± 0.01	19.78 ± 0.01	19.60 ± 0.022	19.32 ± 0.05	19.05 ± 0.07	18.52 ± 0.14
0.648	20.31 ± 0.01	19.99 ± 0.01	19.77 ± 0.02	19.56 ± 0.021	19.40 ± 0.06	19.12 ± 0.08	18.85 ± 0.17
0.657	20.30 ± 0.01	19.99 ± 0.01	19.79 ± 0.02	19.62 ± 0.021	19.29 ± 0.06	19.10 ± 0.08	18.70 ± 0.15
0.666	20.36 ± 0.01	20.01 ± 0.01	19.85 ± 0.01	19.61 ± 0.023	19.34 ± 0.06	19.03 ± 0.07	18.66 ± 0.15
0.675	20.33 ± 0.01	20.04 ± 0.01	19.81 ± 0.02	19.62 ± 0.021	19.37 ± 0.06	19.14 ± 0.08	18.55 ± 0.13
0.684	20.37 ± 0.01	20.05 ± 0.01	19.85 ± 0.02	19.65 ± 0.018	19.47 ± 0.06	19.16 ± 0.07	18.47 ± 0.12
0.693	20.37 ± 0.01	20.05 ± 0.01	19.87 ± 0.02	19.68 ± 0.022	19.48 ± 0.06	19.16 ± 0.07	18.79 ± 0.16
0.702	20.36 ± 0.02	20.06 ± 0.01	19.88 ± 0.02	19.68 ± 0.023	19.49 ± 0.06	19.22 ± 0.07	18.91 ± 0.16
0.709	–	–	–	–	19.50 ± 0.09	19.33 ± 0.11	18.82 ± 0.19
0.714	–	–	–	–	19.47 ± 0.09	19.26 ± 0.12	19.03 ± 0.26
0.719	–	–	–	–	19.59 ± 0.10	19.16 ± 0.10	18.75 ± 0.18
0.724	–	–	–	–	19.36 ± 0.10	19.15 ± 0.10	18.72 ± 0.18
0.728	–	–	–	–	19.58 ± 0.18	19.24 ± 0.11	18.97 ± 0.23
1.700	21.63 ± 0.05	21.32 ± 0.03	21.09 ± 0.06	20.81 ± 0.07	20.73 ± 0.18	20.51 ± 0.23	19.96 ± 0.31
2.626	22.37 ± 0.05	22.01 ± 0.04	21.72 ± 0.06	21.59 ± 0.07	>21.60	>21.15	>19.93
3.707	23.25 ± 0.27	22.65 ± 0.12	22.01 ± 0.18	22.41 ± 0.26	>21.27	>20.76	>20.14
5.686	23.73 ± 0.09	23.20 ± 0.06	22.69 ± 0.09	22.51 ± 0.09	>21.65	>21.15	>20.09
7.675	24.08 ± 0.16	23.68 ± 0.11	23.02 ± 0.15	22.95 ± 0.17	>21.64	>21.16	>20.04
18.654	24.54 ± 0.30	24.08 ± 0.16	23.27 ± 0.13	22.95 ± 0.10	>22.35	>21.80	>20.89
25.669	24.96 ± 0.23	24.17 ± 0.12	23.61 ± 0.18	23.29 ± 0.16	>22.26	>21.78	>20.91
59.538	25.12 ± 0.26	24.33 ± 0.13	23.72 ± 0.21	23.40 ± 0.21	>22.23	>21.82	>20.52
89.434	25.50 ± 0.31	24.40 ± 0.18	24.01 ± 0.22	23.29 ± 0.15	>22.28	>21.68	>20.60
1499.564	25.16 ± 0.17	24.52 ± 0.12	24.04 ± 0.14	23.80 ± 0.20	> 22.34	>21.84	>20.74

Notes. $t - t_0$ is the time in units of days after the burst (t_0 = 28 December 2011, 15:44:43 UT; Ukwatta et al. 2011). The data are not corrected for Galactic extinction.

Table C.8. GRB 111228A: UVOT AB mags (not corrected for Galactic extinction) and upper limits.

$t - t_0$	exp	mag	Filter	$t - t_0$	exp	mag	Filter	$t - t_0$	exp	mag	Filter
0.00433	19.5	$19.35^{+0.35}_{-0.26}$	*uvw2*	5.58389	2477.5	$23.73^{+0.91}_{-0.49}$	*uvw1*	0.00185	10.0	$18.44^{+0.14}_{-0.13}$	white
0.00634	19.4	$18.59^{+0.23}_{-0.19}$	*uvw2*	6.16284	1605.3	>22.53	*uvw1*	0.00197	10.0	$18.29^{+0.13}_{-0.12}$	white
0.00839	19.4	$18.89^{+0.27}_{-0.22}$	*uvw2*	0.00547	19.4	$17.72^{+0.15}_{-0.13}$	*u*	0.00208	10.0	$18.17^{+0.12}_{-0.11}$	white
0.01190	19.5	$18.95^{+0.29}_{-0.23}$	*uvw2*	0.00749	19.5	$18.00^{+0.17}_{-0.15}$	*u*	0.00220	10.0	$18.04^{+0.11}_{-0.10}$	white
0.01390	19.5	$18.66^{+0.25}_{-0.20}$	*uvw2*	0.00952	19.4	$17.99^{+0.18}_{-0.16}$	*u*	0.00231	10.0	$18.17^{+0.12}_{-0.11}$	white
0.07245	196.6	$19.60^{+0.12}_{-0.10}$	*uvw2*	0.01303	16.6	$18.18^{+0.28}_{-0.22}$	*u*	0.00243	10.0	$18.02^{+0.11}_{-0.10}$	white
0.13358	885.6	$20.02^{+0.07}_{-0.06}$	*uvw2*	0.06532	196.6	$18.42^{+0.07}_{-0.06}$	*u*	0.00255	10.0	$18.11^{+0.12}_{-0.11}$	white
0.52521	804.9	$21.84^{+0.20}_{-0.17}$	*uvw2*	0.08107	47.7	$18.27^{+0.18}_{-0.16}$	*u*	0.00266	10.0	$18.20^{+0.12}_{-0.11}$	white
0.72515	885.6	$21.82^{+0.19}_{-0.16}$	*uvw2*	0.11799	30.1	$18.74^{+0.22}_{-0.18}$	*u*	0.00278	10.0	$17.92^{+0.11}_{-0.10}$	white
1.83617	1209.7	$23.45^{+0.59}_{-0.38}$	*uvw2*	0.47818	746.5	$20.22^{+0.12}_{-0.11}$	*u*	0.00289	10.0	$18.03^{+0.11}_{-0.10}$	white
2.73793	1123.3	>22.48	*uvw2*	0.66585	275.5	$20.73^{+0.26}_{-0.21}$	*u*	0.00301	10.0	$18.06^{+0.12}_{-0.10}$	white
3.56617	1674.5	$23.81^{+0.63}_{-0.40}$	*uvw2*	0.87038	885.1	$21.23^{+0.21}_{-0.17}$	*u*	0.00312	10.0	$17.93^{+0.11}_{-0.10}$	white
4.73622	2169.3	>22.66	*uvw2*	0.94385	292.4	$21.14^{+0.38}_{-0.28}$	*u*	0.00324	10.0	$17.94^{+0.11}_{-0.10}$	white
6.72761	5232.4	>22.75	*uvw2*	1.23909	1036.5	$21.62^{+0.27}_{-0.21}$	*u*	0.00336	10.0	$17.92^{+0.11}_{-0.10}$	white
8.33080	2974.9	>22.62	*uvw2*	3.43175	1658.5	>21.60	*u*	0.00347	9.7	$17.95^{+0.11}_{-0.10}$	white
10.2592	7029.7	>22.80	*uvw2*	4.60168	1999.8	>21.57	*u*	0.00605	19.4	$17.80^{+0.07}_{-0.07}$	white
12.7314	49449.0	>25.00	*uvw2*∗	6.60718	3520.6	>21.61	*u*	0.00807	19.5	$18.09^{+0.09}_{-0.08}$	white
14.6397	3521.2	>22.84	*uvw2*	7.63888	15759.0	>23.60	*u*∗	0.01081	147.4	$18.05^{+0.04}_{-0.04}$	white
19.8672	25310.8	>22.96	*uvw2*	8.26114	2625.5	>21.41	*u*	0.01361	19.4	$18.24^{+0.12}_{-0.11}$	white
22.2613	1252.6	>22.65	*uvw2*	10.9366	5174.4	>21.81	*u*	0.07006	196.6	$18.70^{+0.05}_{-0.05}$	white
0.00491	19.5	$18.17^{+0.25}_{-0.20}$	*uvm2*	12.1980	3912.1	>22.52	*u*	0.59775	164.3	$21.05^{+0.21}_{-0.18}$	white
0.00693	19.5	$18.43^{+0.28}_{-0.22}$	*uvm2*	0.00576	19.4	$17.52^{+0.19}_{-0.16}$	*b*	0.80219	817.4	$21.21^{+0.10}_{-0.09}$	white
0.00896	19.4	$18.49^{+0.30}_{-0.23}$	*uvm2*	0.00779	19.5	$17.42^{+0.18}_{-0.15}$	*b*	1.87291	885.1	$22.48^{+0.33}_{-0.25}$	white
0.01246	19.5	$18.69^{+0.33}_{-0.25}$	*uvm2*	0.00981	19.4	$17.61^{+0.22}_{-0.19}$	*b*	3.14088	1236.5	$23.45^{+0.79}_{-0.45}$	white
0.01446	19.5	$18.46^{+0.29}_{-0.23}$	*uvm2*	0.01332	19.4	$17.74^{+0.32}_{-0.25}$	*b*	4.47754	2421.9	$23.63^{+0.61}_{-0.39}$	white
0.07719	196.6	$19.25^{+0.13}_{-0.11}$	*uvm2*	0.06769	196.6	$18.22^{+0.08}_{-0.08}$	*b*	6.74437	4351.5	>22.19	white
0.26183	248.8	$20.25^{+0.19}_{-0.16}$	*uvm2*	0.21029	822.3	$19.13^{+0.09}_{-0.08}$	*b*	8.75036	2143.0	>22.03	white
0.28021	312.3	$20.76^{+0.25}_{-0.20}$	*uvm2*	0.59146	885.1	$20.71^{+0.28}_{-0.22}$	*b*	11.0237	8490.5	>22.51	white
0.33289	885.6	$20.82^{+0.14}_{-0.12}$	*uvm2*	0.79203	885.2	$20.74^{+0.28}_{-0.22}$	*b*	14.0660	2872.2	>22.27	white
0.92634	885.6	$22.38^{+0.35}_{-0.26}$	*uvm2*	0.87714	244.3	$20.31^{+0.42}_{-0.30}$	*b*	18.5185	61512.0	>25.00	white*
1.14712	682.1	$22.63^{+0.58}_{-0.37}$	*uvm2*	1.21404	664.6	$20.90^{+0.55}_{-0.36}$	*b*	21.6931	15200.1	>22.56	white
1.26110	885.6	$22.09^{+0.29}_{-0.23}$	*uvm2*	2.43093	1292.4	>20.61	*b*	30.5139	18317.7	>22.54	white
2.81012	1688.1	>22.15	*uvm2*	3.50282	1251.3	>20.76	*b*	33.7246	13313.4	>23.09	white
4.34176	2187.1	>22.31	*uvm2*	3.93518	5332.0	>22.20	*b*∗				
4.39814	6573.0	>24.00	*uvm2*∗	4.60650	1999.8	>20.74	*b*				
5.57821	2638.5	>22.27	*uvm2*	5.92886	1577.8	>20.90	*b*				
6.16084	1666.1	>22.97	*uvm2*	0.00161	10.6	$18.14^{+1.04}_{-0.52}$	*v*				
0.00519	19.4	$18.04^{+0.19}_{-0.16}$	*uvw1*	0.00462	19.5	$18.10^{+0.66}_{-0.41}$	*v*				
0.00721	19.4	$18.53^{+0.25}_{-0.21}$	*uvw1*	0.00665	19.5	$17.82^{+0.50}_{-0.34}$	*v*				
0.00924	19.4	$8.46^{+0.25}_{-0.20}$	*uvw1*	0.00867	19.5	$17.14^{+0.29}_{-0.23}$	*v*				
0.01275	19.5	$18.76^{+0.31}_{-0.24}$	*uvw1*	0.01218	19.5	$17.18^{+0.37}_{-0.27}$	*v*				
0.01464	1.7	$18.68^{+2.31}_{-0.69}$	*uvw1*	0.01418	19.4	$17.61^{+0.63}_{-0.39}$	*v*				
0.05120	49.6	$18.78^{+0.17}_{-0.15}$	*uvw1*	0.07482	196.6	$18.17^{+0.15}_{-0.13}$	*v*				
0.06295	196.6	$18.82^{+0.09}_{-0.08}$	*uvw1*	0.14359	792.7	$18.61^{+0.12}_{-0.11}$	*v*				
0.07957	196.6	$19.02^{+0.11}_{-0.10}$	*uvw1*	0.54557	656.2	$20.43^{+0.81}_{-0.46}$	*v*				

Notes. Midtimes are derived logarithmically, $t = 10^{([log(t_1-t_0)+log(t_2-t_0)]/2)}$, hereby $t_{1,2}$ are the start and stop times, t_0 is the *Swift* trigger time. Upper limits marked with a ∗ represent stacks of all observations in each specific filter that yielded only upper limits, to obtain deeper limits on the host galaxy.

Table C.8. continued.

$t - t_0$	exp	mag	Filter	$t - t_0$	exp	mag	Filter	$t - t_0$	exp	mag	Filter
0.34185	622.0	$20.44^{+0.13}_{-0.12}$	*uvw1*	0.73368	545.8	$20.44^{+0.67}_{-0.41}$	*v*				
0.64009	900.8	$21.41^{+0.19}_{-0.16}$	*uvw1*	1.46837	1180.2	>19.68	*v*				
0.85984	885.6	$21.49^{+0.20}_{-0.17}$	*uvw1*	2.40912	891.7	>19.69	*v*				
0.93684	885.6	$21.74^{+0.24}_{-0.20}$	*uvw1*	3.51254	1157.7	>19.85	*v*				
1.23288	1771.2	$22.16^{+0.22}_{-0.18}$	*uvw1*	3.93518	4958.0	>21.30	*v*∗				
2.81533	1544.0	$22.84^{+0.48}_{-0.33}$	*uvw1*	4.54936	1494.0	>19.84	*v*				
4.34832	2008.8	>22.09	*uvw1*	5.58572	1119.1	>19.83	*v*				
5.09259	4582.0	>23.50	*uvw1*∗	5.98716	739.8	>20.23	*v*				

Table C.9. GRB 120714B: GROND AB magnitudes and upper limits of the optical transient.

$t - t_0$	g'	r'	i'	z'	J	H	K_s
0.265	22.43 ± 0.07	22.09 ± 0.07	22.33 ± 0.16	21.65 ± 0.13	>21.04	>20.51	>19.94
0.354	22.49 ± 0.06	22.19 ± 0.05	22.18 ± 0.08	21.78 ± 0.08	–	–	–
0.375	22.44 ± 0.05	22.21 ± 0.05	22.27 ± 0.10	21.97 ± 0.10	–	–	–
0.396	22.40 ± 0.05	22.23 ± 0.05	22.12 ± 0.09	21.86 ± 0.09	21.75 ± 0.17	>21.72	>21.32
0.417	22.39 ± 0.04	22.24 ± 0.05	22.11 ± 0.09	–	–	–	–
0.438	22.44 ± 0.05	22.18 ± 0.05	22.32 ± 0.11	21.90 ± 0.10	–	–	–
1.480	22.94 ± 0.08	22.48 ± 0.07	22.35 ± 0.15	22.36 ± 0.12	>22.10	>21.53	>20.95
2.488	23.33 ± 0.10	22.49 ± 0.08	22.52 ± 0.13	22.28 ± 0.13	>21.96	>21.43	>20.08
4.511	23.40 ± 0.20	22.47 ± 0.10	–	22.06 ± 0.14	>21.86	>21.31	>19.50
7.391	23.49 ± 0.09	22.28 ± 0.06	22.15 ± 0.10	22.00 ± 0.11	>21.75	> 20.95	>20.28
9.471	23.55 ± 0.10	22.28 ± 0.05	22.02 ± 0.09	22.18 ± 0.09	>22.37	>21.77	>20.39
12.469	–	22.24 ± 0.05	21.95 ± 0.09	21.91 ± 0.10	>22.27	>21.63	>20.09
15.511	23.68 ± 0.14	22.31 ± 0.07	21.89 ± 0.10	21.82 ± 0.12	>21.59	>20.91	>20.27
24.432	23.70 ± 0.20	22.53 ± 0.06	21.86 ± 0.06	21.81 ± 0.08	>21.97	>21.43	>20.55
26.380	23.74 ± 0.12	22.49 ± 0.06	21.88 ± 0.07	21.74 ± 0.07	>22.04	>21.42	>20.24
41.391	23.72 ± 0.10	22.68 ± 0.06	22.20 ± 0.09	22.10 ± 0.11	>22.27	>21.59	>20.77
97.244	23.77 ± 0.10	22.86 ± 0.08	22.55 ± 0.10	22.57 ± 0.11	>22.39	>21.77	>20.79
144.166	23.88 ± 0.13	22.80 ± 0.09	22.86 ± 0.14	22.44 ± 0.14	>21.97	>21.50	>20.66
449.274	23.83 ± 0.13	22.95 ± 0.10	22.72 ± 0.10	22.52 ± 0.12	>21.75	>21.12	–

Notes. $t - t_0$ is the time in units of days after the burst (t_0 = 14 July 2012, 21:18:47 UT; Saxton et al. 2012). The data are not corrected for Galactic extinction.

Table C.10. GRB 130831A: GROND AB magnitudes and upper limits of the optical transient.

$t - t_0$	g'	r'	i'	z'	J	H	K_s
0.618	20.30 ± 0.12	20.09 ± 0.13	19.85 ± 0.14	19.58 ± 0.16	>19.46	>18.59	>18.16
0.639	20.55 ± 0.08	20.17 ± 0.10	19.92 ± 0.10	19.65 ± 0.09	>20.00	>19.22	–
0.665	20.52 ± 0.07	20.19 ± 0.08	19.93 ± 0.12	19.74 ± 0.08	19.40 ± 0.13	18.96 ± 0.19	–
0.689	20.60 ± 0.03	20.35 ± 0.04	20.10 ± 0.04	19.89 ± 0.05	19.50 ± 0.08	19.25 ± 0.12	18.55 ± 0.12
0.714	20.73 ± 0.02	20.35 ± 0.03	20.16 ± 0.03	19.97 ± 0.04	19.48 ± 0.06	19.15 ± 0.09	19.11 ± 0.14
0.736	–	20.43 ± 0.06	20.16 ± 0.08	19.96 ± 0.10	19.68 ± 0.20	>19.49	>18.54
0.762	–	–	–	–	>19.78	–	–
1.645	21.98 ± 0.07	21.80 ± 0.08	21.76 ± 0.12	21.56 ± 0.14	>21.32	>20.50	–
1.689	22.01 ± 0.05	21.85 ± 0.05	21.81 ± 0.10	21.66 ± 0.12	>21.63	>20.98	–
1.736	22.05 ± 0.05	21.80 ± 0.05	21.85 ± 0.08	21.82 ± 0.13	>21.61	>20.92	–
2.624	22.59 ± 0.05	22.38 ± 0.06	22.25 ± 0.11	22.42 ± 0.15	>21.80	>20.73	>20.23
3.724	23.00 ± 0.14	22.59 ± 0.11	22.91 ± 0.33	22.46 ± 0.22	>21.25	>20.28	–
7.712	23.36 ± 0.11	22.95 ± 0.09	22.62 ± 0.12	22.88 ± 0.20	>22.04	>21.07	>19.94
11.663	23.56 ± 0.16	23.05 ± 0.13	22.72 ± 0.18	22.80 ± 0.15	>22.20	>21.07	>20.52
24.606	24.56 ± 0.29	23.22 ± 0.13	22.75 ± 0.15	22.98 ± 0.19	>22.07	>20.86	–
29.598	>24.60	23.58 ± 0.21	23.18 ± 0.19	23.09 ± 0.19	>21.99	>21.11	>20.49
33.622	24.81 ± 0.22	23.67 ± 0.16	23.48 ± 0.17	23.12 ± 0.12	>22.71	>22.00	>21.09
386.643	24.86 ± 0.27	24.21 ± 0.17	>24.25	23.76 ± 0.30	–	–	–

Notes. $t - t_0$ is the time in units of days after the burst (t_0 = 31 August 2013, 13:04:16 UT; Hagen et al. 2013). The data are not corrected for Galactic extinction.

Table C.11. Additional data not based on GROND observations.

GRB	Band	Time (days)	AB magnitude	Telescope
071112C	B	2189	25.99 ± 0.12	Keck/LRIS
	g'	1763	26.06 ± 0.06	Gemini North/GMOS
	r'	290	25.47 ± 0.11	Gemini North/GMOS
	R_c	2189	25.43 ± 0.18	Keck/LRIS
	3.6 μm	1826	23.59 ± 0.11	*Spitzer*/IRAC
111228A	R_c	29.33	24.08 ± 0.16	TNG/DoLoRes
	R_c	34.51	24.12 ± 0.13	TNG/DoLoRes
	R_c	76.23	24.53 ± 0.22	TNG/DoLoRes
	I_c	34.44	23.33 ± 0.10	TNG/DoLoRes
	I_c	76.30	24.10 ± 0.14	TNG/DoLoRes
120714B	J	455	22.34 ± 0.13	VLT/HAWKI
	K_s	455	22.22 ± 0.14	VLT/HAWKI
130831A	J	289	23.53 ± 0.22	Keck/MOSFIRE
	3.6 μm	756	>24.0	*Spitzer*/IRAC

Notes. Given magnitudes are not corrected for Galactic extinction. The time refers to how many days after the corresponding burst the data were taken.